Design and Optimization of Anodic Aluminum Oxide Channels Through Anodization of Aluminum Foil

By

Abdul Qadeer

School of Chemical and Materials Engineering (SCME)

National University of Sciences and Technology (NUST)

2017

Design and Optimization of Anodic Aluminum Oxide Channels Through Anodization of Aluminum Foil

Name: Abdul Qadeer

Reg. No: NUST201463831MSCME67714F

This thesis is submitted as a partial fulfillment of the requirements for the degree of

(MS in Materials and Surface Engineering)

Supervisor Name: Dr. Zakir Hussain

School of Chemical and Materials Engineering (SCME)

National University of Sciences and Technology (NUST),

H-12 Islamabad, Pakistan

January, 2017

In the Name of Allāh, the Most Gracious, the Most Merciful

Dedication

This Work is dedicated to
my Loving Family

"I could'nt have done without them"

Acknowledgment

"*Truly, my prayer and my service of sacrifice, my life and my death are for Allah, the cherisher of the worlds*" (Surah Al-Anaam 6:162) Al-Quran.

I am thankful to Allah who gave me strength to complete this MS thesis work. Without His will, nothing is possible.

I would like to thank my family especially my mother who always prays for me. She gave confidence to me every time I failed to proceed.

I would like to thank my supervisor **Dr. Zakir Hussain,** co-supervisor **Dr. Haris Ansari** and GEC members **Dr. Mohammad Mujahid** and **Dr. Iftikhar Hussain Gul** for continuous support and unremitting technical guideline to complete this thesis.

I wholly recognize all faculty members, technical staff, nonteaching staff especially **Mr. Shamshuddin** for SEM and my fellow students for the assistance provided to me throughout this research work.

Abdul Qadeer

Abstract

TEM gold grids act as sensing chambers for liquid crystal based sensing applications, which are expensive. Anodized aluminum oxide (AAO) channels can replace these chambers and can help in performing multiple sensing on one substrate. In this research work, impure aluminum foil is used to study and optimize the AAO channels through anodization because of cost effectiveness and ease of fabrication. Stepwise anodization is performed by varying voltage and working temperature for nine set of experiments to increase the pore size of AAO channels. Anodization process was monitored to make current profiles that are a function of current and time to predict and analyze the mechanism of pores. The process of high voltage anodization produces local heat at the surface of aluminum foil which was reduced by maintaining low working temperatures of anodization bath and also with continuous stirring of electrolyte. Scanning electron microscopy was used to investigate surface morphology and cross sectional analysis of anodized aluminum oxide channels for each set of experiment. This research work resulted in formation of AAO channels with pore size ranging from 40-270 nm and length of 1-17 μm through optimized two-step anodization of impure aluminum foil performed in 5-vol % phosphoric acid at anodizing voltage of 40-190 V.

Table of Contents

List of Figures

List of Tables

Abbreviations

PAA	Porous Anodic Alumina
AAO	Anodic Aluminum Oxide
SEM	Scanning Electron Microscope
AFM	Atomic Force Microscope
EDS	Energy Dispersive Spectroscopy
DC	Direct Current
DMM	Digital Multi-meter
PEG	Poly Ethylene Glycol
LC	Liquid Crystal
AO	Anodization in Oxalic acid
AP	Anodization in Phosphoric acid
A	Anodization
TEM	Transmission Electron Microscopy

Chapter 1

Introduction

1.1. Anodization of aluminum

The anodization of aluminum is an electrochemical process to produce protective and decorative coatings on aluminum substrates. A positive constant voltage is applied to an aluminum foil, sheet or film in an acidic electrolyte, which results in the formation of an oxide layer on the surface of aluminum [1]. This oxide layer formed on the surface of aluminum is known as anodized aluminum oxide (AAO) and has hexagonal structure as shown in Figure 1.1 that was successfully revealed by Keller et al. [2] in 1953.

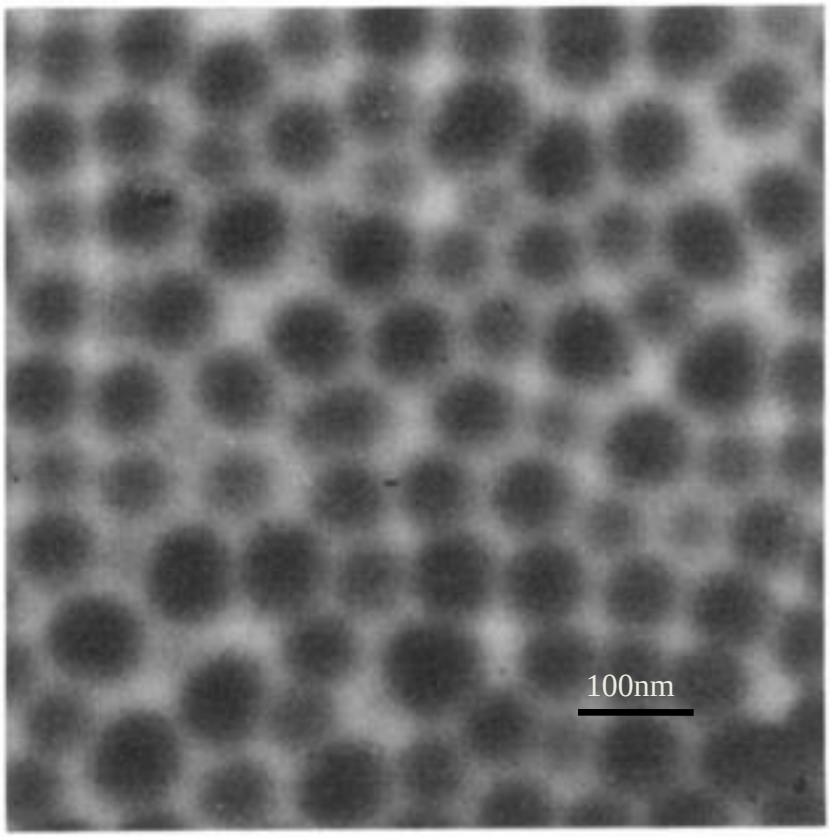

Figure 1.1. TEM image of hexagonal structure of AAO obtained in phosphoric acid at 120 V [2].

The structural features of AAO can be optimized easily by varying the parameters of anodization [3]. In 1995, Masuda et al. [4] fabricated honeycomb structure of anodized aluminum oxide by two step anodization process. By slight changes in anodization parameters, various templates of AAO can be obtained on aluminum to use them in number of applications such as protective coatings [5], solar cells [6], power storage [7-9], separation membranes [10], bio-sensing [11, 12], wetting [13] and magnetic applications [14, 15].

1.2. Anodic aluminum oxide channels and effects of anodization parameters on the aluminum

Anodization of aluminum foil can be performed in acidic solutions like sulfuric acid, oxalic acid and phosphoric acid [16], and the most common electrolyte to obtain pores, is sulfuric acid [17]. The selection of electrolyte depends on final application and pore size of channels. The more bigger pores need concentrated acidic solutions [18], while small and regular pores of AAO can be obtained by using sulfuric acid at low working temperatures [19, 20]. The anodization parameters define the final morphology of the anodic aluminum oxide channels. The anodization performed in dilute acidic electrolyte at constant anodic voltage is known as potentiostatic anodization [21] while anodization performed at constant anodic current is known as galvanostatic anodization [22]. Generally, the potentiostatic condition is used to carry out anodization in the range of 10-15 V for sulfuric acid [23, 24], 25-40 V for oxalic acid [25] and 60-195V for phosphoric acid [26]. Anodic aluminum oxide channels produced in sulfuric acid have low flexibility, less surface hardness, and good scratch resistance. Local heat on the surface of aluminum is generated during high voltage anodization that can be compensated by using low working temperatures. However, at low working temperatures anodization results in thick, compact and hard oxide layer [27]. It is reported by researchers that every parameter holds its importance and can affect the final morphology of anodic aluminum oxide channels by variation in any anodizing parameter [28-30]. Moreover, the final pore size and height of channels depends on the electrolyte, working temperature, applied voltage, thickness of sample, local heat, anodization time and

pretreatments. Among all, the applied voltage has linear relation with final pore size of anodic aluminum oxide channels [31]. A huge growth is seen in research publications from 1990 to 2015 [32] for anodic aluminum oxide channels as shown in Figure 1.2.

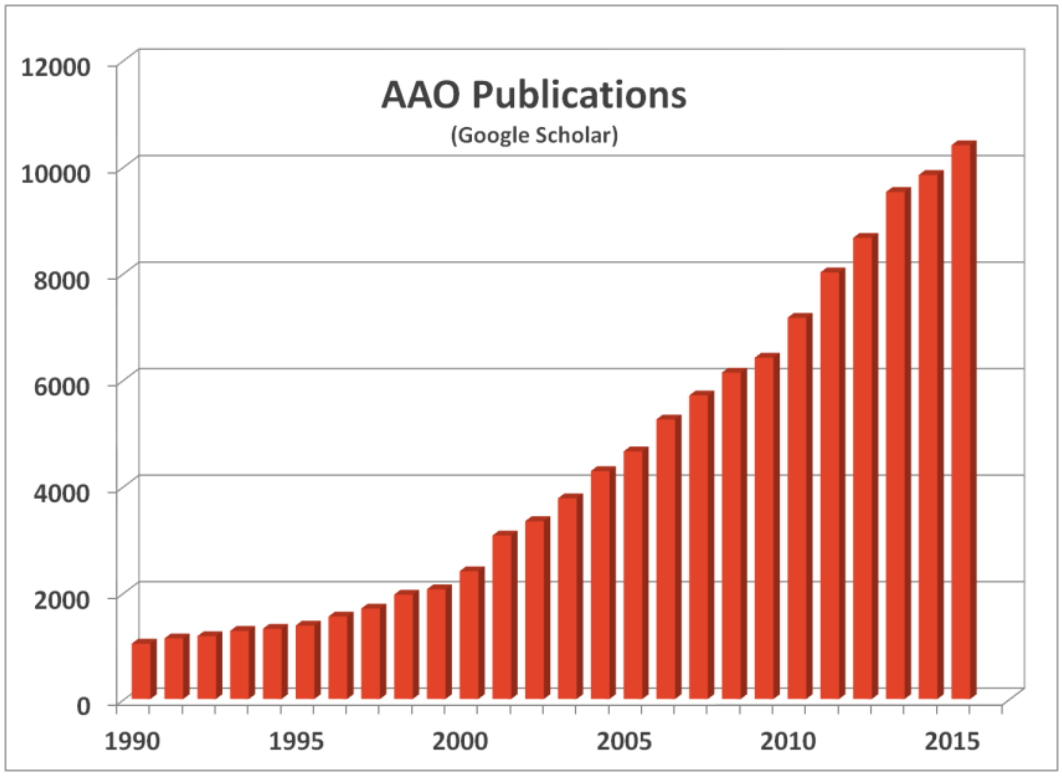

Figure 1.2. Growth in research publications of AAO from 1990 to 2015 [32].

1.3. Electrochemical reactions

There are numerous electrochemical techniques such as electro-deposition [33], electro-polishing [34, 35], electro-etching [36], anodization [37, 38], pitting [39, 40] and corrosion protections [41]. However, for electrochemical reactions, presence of four components is important that make the electrochemical cell and if any of the component is absent, the reaction will not start. The main four components are given as [42, 43]:

i. Anode
ii. Cathode
iii. Electrolyte (for ionic conduction)
iv. Electrical connection between anode and cathode (for flow of electron current)

1.3.1. Electro-deposition

In electro-deposition, inert electrode such as graphite or lead is used as an anode, while the metal on which the deposition is required is used as cathode. Positive ions from electrolyte are deposited on the surface of cathode and hence deposition is achieved on the metal. The schematic of electro-deposition is shown in Figure 1.3.

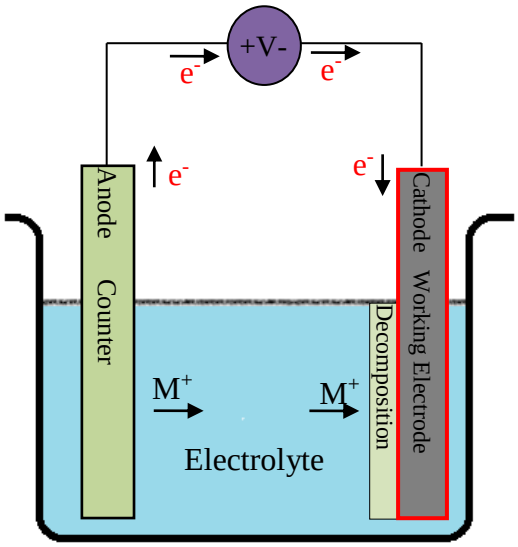

Figure 1.3. Electro-deposition [44].

1.3.2. Electro-etching

In this electrochemical process, sample is attached to the positive terminal of the DC power supply. Positive ions are discharged from the surface of a sample, which acts as an anode, to the electrolyte while the electrons reach to the cathode through the electrical connection of an electrochemical cell. The mechanism of electro-etching is presented in Figure 1.4.

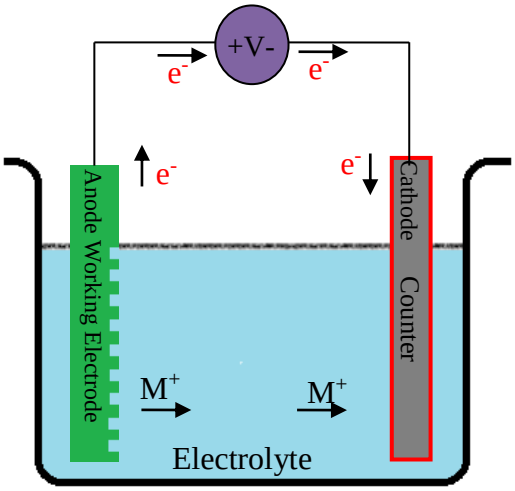

Figure 1.4. Electro-etching [44].

1.3.3. Electro-polishing

The sample acts as an anode while an inert electrode acts as a cathode. Concentrated acidic electrolytes are used for the electro-polishing, in which metallic surface oxidizes and dissolves into the electrolyte and hence the electro-polishing is achieved on sample. The mechanism is shown in Figure 1.5.

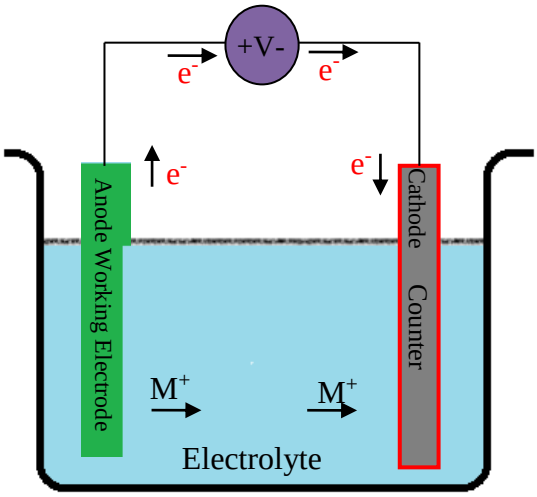

Figure 1.5. Electro-polishing [44].

1.3.4. Anodization

Working electrode is an anode while cathode acts as a counter electrode that receives electrons from the anode through electrical connection. The electrolyte has the negative charged ions, which will move towards the anode [10, 38] and form an oxide layer on the surface of anode. In case of aluminum as an anode, this oxide is known as anodized aluminum oxide [30]. The mechanism of electrochemical anodization is depicted in Figure 1.6.

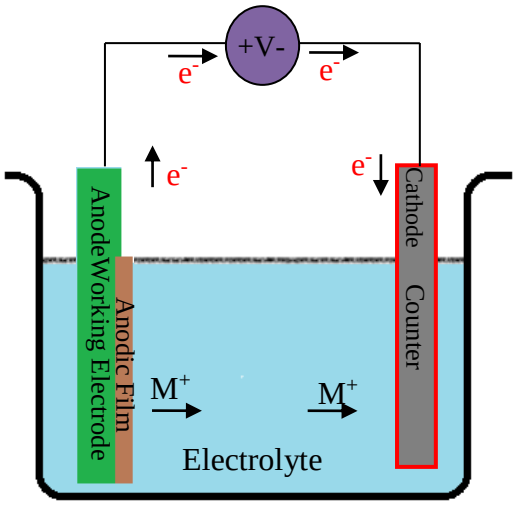

Figure 1.6. Anodization [44].

1.3.5. Pitting

It is a localized form of corrosion that results in the form of cavities and holes in the metal. It is one of the most destructive and insidious form of corrosion which is considered to be more hazardous than uniform corrosion because it is difficult to detect and predict [45].

1.3.6. Corrosion protection

It is a preventive technique to protect the surface of metals by making that surface cathode of an electrochemical cell. The major two types of corrosion protection are; sacrificial anode cathodic protection and impressed current cathodic protection [41].

1.4. Liquid crystals

A substance that flows like a liquid and has some degree of ordering in the arrangement of its molecules, is called liquid crystal.

Liquid crystals are intermediate between the solid and liquid phase. It can flow like a liquid and at the same time, it can behave like a solid. So, in brief terms it has flow ability and has degree of order in arrangement of molecules, which act as a solid. It has anisotropic, electrical, optical [46], magnetic properties and fluidity; so it is an intermediate state of matter having functions of solid and liquid at the same time [46].

1.4.1. Phases of liquid crystals

On the basis of ordering, temperature, concentration, organic and inorganic molecules, the major phases of liquid crystals are:

1.4.1.1.Lyotropic

Liquid crystals, which show phase change in response to change in temperature and concentration are termed as lyotropic liquid crystals [47].

1.4.1.2.Metallotropic

The liquid crystals having organic-inorgainc ratio of molecules at low temperature are classified as metallotropic liquid crystals [47].

1.4.1.3. Thermotropic

These liquid crystals have different phases in different ranges of temperature. Among above phases, thermotropic phase is significant because it totally depends on the temperature and it transforms to other phases at different temperatures. It is subdivided into more phases which are briefly described as follows [47]:

a. Nematic phase

Nematic is derived from its Greek meaning “Thread”; it is translucent and transparent which causes the polarization of liquid crystals. The liquid molecules align themselves into a thread like orientation.

b. Smectic Phase

This word derived from Latin, which means to clean, or of soapy nature. Their layers are well defined when observed at temperatures lower than nematic phases.

c. Cholestric phase

Due to the presence of chiral molecules there is a twist in nematic phase. Such a twisted helical phase is known as cholestric liquid crystal phase. There are quasi-nematic layers in cholesteric liquid crystals but layers are present at some definite angle.

1.4.2. Alignment of liquid crystals

There are two types of alignments found in liquid crystal molecules, namely as homogeneous alignment and homeotropic alignment. Both are briefly explained as below:

a. Homogenous alignment

When the molecules of liquid crystals align themselves parallel to the substrate then alignment is said to be homogenous alignment.

b. Homeotropic alignment

When the molecules of liquid crystals align themselves perpendicular to the substrate then alignment is said to be homeotropic alignment.

1.5. Liquid crystal sensors

Liquid crystals are responsive to the foreign molecules, voltage and light. This responsive nature of LC molecules is used for sensing applications. 4 cyano – 4 pentyl bi phenyl ($C_{18}H_{18}N$), displays a nematic mesophase, commonly known as 5CB and is widely used in electro-optic display and sensing devices. N – dimethyl – N – octyl – N – 3-trimethoxy silyl propyl ammonium chloride (DMOAP) is used as surfactant to obtain homeotropic alignment. The function of surfactant is to provide an alignment layer on glass substrate. TEM Gold grids provide the confinement chambers to LC molecules. The liquid crystal molecules are smeared uniformly in 20-µm thick TEM grids having 150-µm cell diameters as shown in Figure 1.7. The liquid crystal form stable freestanding films in each grid cell.

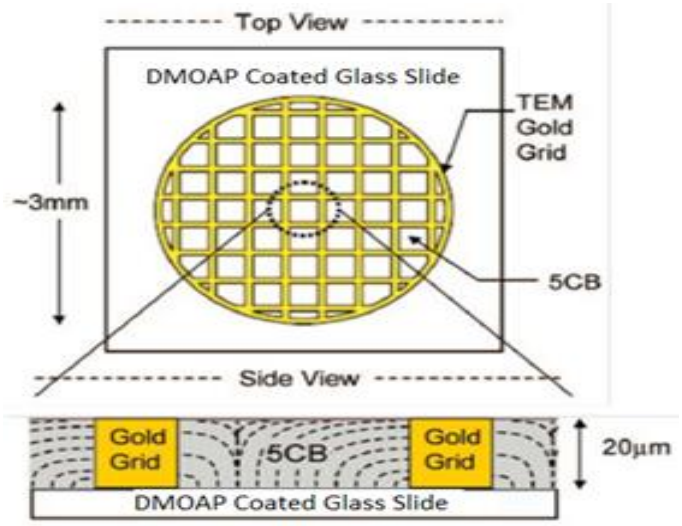

Figure 1.7. TEM gold grids used for LC based sensing applications [48].

Liquid crystal sensing is performed by applying LC molecules on DMOAP coated glass substrate having TEM grids as confinement chambers and then glass substrate is observed under polarized optical microscope. There would be some leakage of light when LC molecules are not aligned in perpendicular direction as shown in Figure 1.8 (a). The leakage of light due to non-alignment of LC molecules is observed from optical microscope as shown in Figure 1.8 (b). Annealing of LC molecules is performed at 40^{o}C to get homeotropic alignment as shown in Figure 1.8 (c) and now the light is completely blocked as shown in Figure 1.8 (d). The orientation of LC

molecules is responsive to any foreign molecule. When foreign substance is applied on the substrate, the alignment can be disturbed and the amount of disruption will be directly proportional to the amplification of optical signal. This disruption of light due to presence of foreign molecule is basis of LC based sensing.

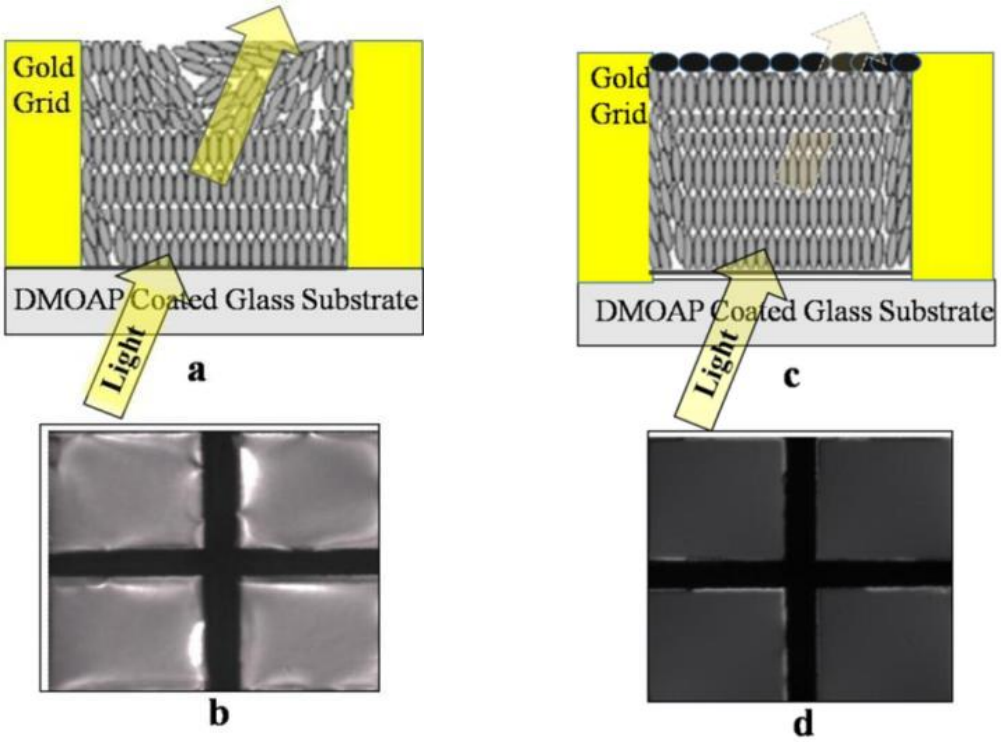

Figure 1.8. Principle of liquid crystal sensor (a) light allowed due to partial alignment of LC molecules (b) observation of light transmittance under optical microscope (c) light completely blocked due to complete alignment of LC molecules (d) light blocked and appeared black in optical microscope [48].

1.6. Anodisc ® whatman alumina

It is commercially available membrane having AAO channels with pore size 200 nm that is mostly used as filtration membrane for specialized applications like HPLC mobile phase filtration and bacterial analysis by light microscopy.

1.7. Problem statement

TEM Gold grids are being used in sensing applications as sensing chambers for liquid crystal molecules and require functionalization of DMOAP; that makes them costly and sophisticated [49]. They are labile and should be replaced with any robust and cheap sensing chamber. One of the best solutions suggested by Hussain et al [48]; is anodized aluminum oxide channels for replacement of TEM grids. This research work is dedicated to design and optimize the anodization setup and to exploit the self-ordering of anodic aluminum oxide channels through anodization on aluminum foil.

Chapter 2

Literature Review

Peter et al. [50] have studied anodization of aluminum in different electrolytes to observe the corrosion protection behavior of alumina with the help of scanning electron microscopy and potentiostatic tafel scans. Samples which were anodized in sulfuric acid gave the better protection against corrosion than samples anodized in other electrolytes. Porous anodic aluminum oxide templates were prepared by Parang et al. [20] in which three different electrolytes; sulfuric, oxalic and phosphoric acids were used separately as well as in mixed conditions. Small pore diameters were obtained in sulfuric acid, while oxalic acid and phosphoric acid gave large size AAO pores. The surface morphology and processing conditions to get ordered cylindrical channels were discussed by Jessensky et al. [51] and anodization was concluded to be self-organized process for oxalic acid compared to anodization performed in sulfuric acid as shown in Figure 2.1.

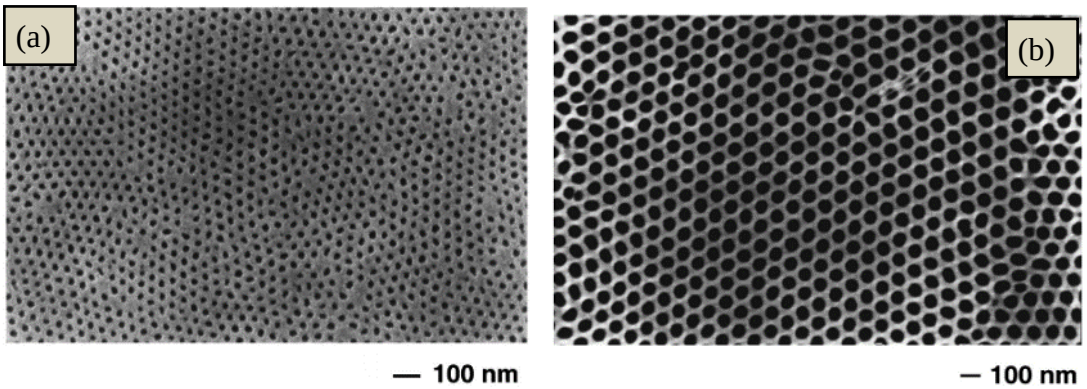

Figure 2.1. Comparison of regularity of hexagonal pore structure of AAO in two electrolytes (a) SEM bottom surface view of a AAO prepared in sulfuric acid (18.7V, 1^{o}C) (b) SEM bottom surface view of a AAO prepared in oxalic acid (40V, 1^{o}C) [51].

Daniel et al. [52] reported the fabrication of porous anodic alumina (PAA) films from commercially available impure aluminum foil. However, the PAA layers from impure aluminum foil contained smaller pores and less

ordered porous structure than obtained from ultrapure aluminum foils as shown in Figure 2.2 (a).

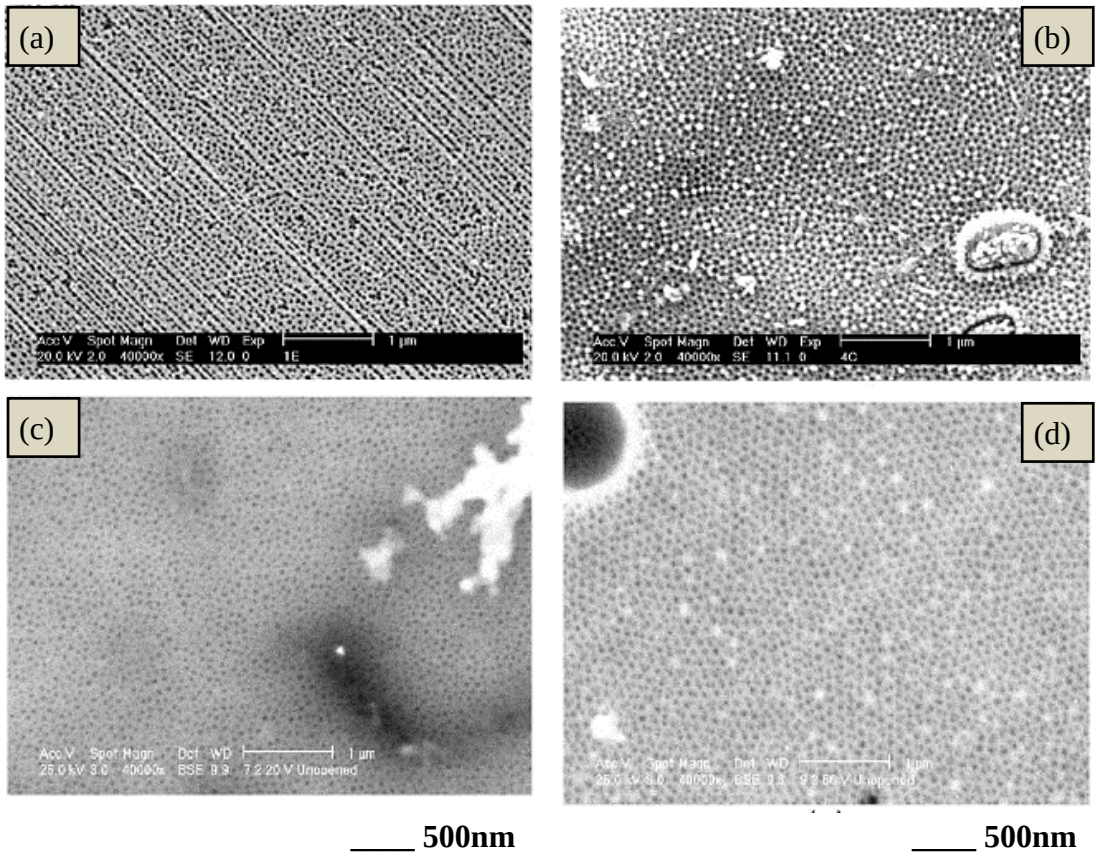

Figure 2.2. SEM micrographs of top surface of PAA films fabricated from impure and ultrapure aluminum foils (a) anodization of impure aluminum foil in 0.3 M oxalic acid with no prior foil annealing (b) anodization of annealed impure aluminum foil in 0.3 M oxalic acid (c) anodization of annealed ultrapure aluminum foil in 0.3 M oxalic acid at 40 V (d) anodization of annealed ultrapure aluminum foil in 0.3 M oxalic acid at 56 V [52].

Daniel et al. [52] also found that regularity of pores, geometric consistency and self-ordering can be increased by prior annealing of impure aluminum foil as shown in Figure 2.2 (b). At 40 V as shown in Figure 2.2 (c) pore ordering is good while at 56 V as shown in Figure 2.2 (d) pores are irregular and showing less hexagonal ordering.

2.1 Pore formation process

The typical anodization process depends on the current profiles that is a function of current and time as depicted in Figure 2.3. It is divided into following four stages:

a. Oxide formation
b. Pore initiation
c. Pore formation
d. Pore growth.

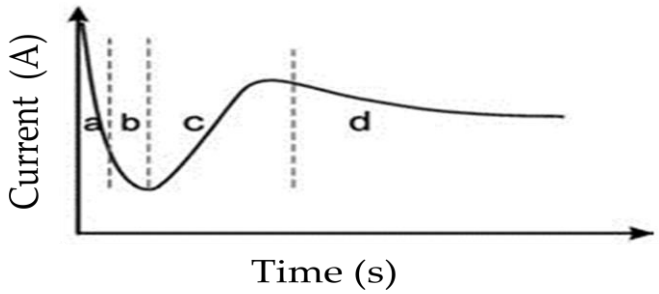

Figure 2.3. Schematic illustration of the kinetics of porous oxide growth in potentiostatic condition [53].

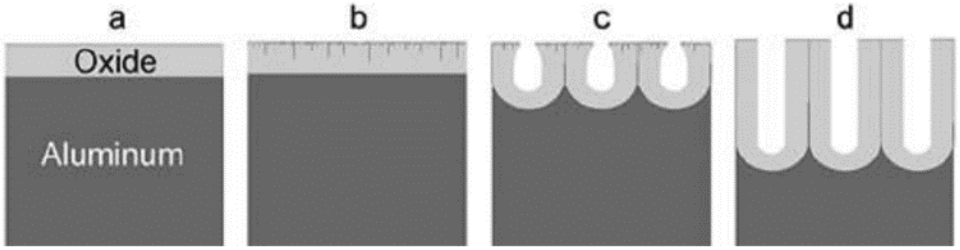

Figure 2.4. Development of porous anodic aluminum oxide channels with stages of pore formation [53].

2.1.1 Stage a: oxide formation

During oxide formation as shown in Figure 2.3 (a) and 2.4 (a), the current density is decreasing with time due to the resistant behavior of oxide film on aluminum. The oxide formation will occur when the current overcomes the resistive oxide layer on aluminum.

2.1.2 Stage b: pore initiation

In this stage as shown in Figure 2.3 (b) and 2.4 (b), the pores precursors are all set to form. The resistance of oxide barrier film reaches its maximum value, and then after it, the pore propagation will start.

2.1.3 Stage c: pore formation

The porous structure starts to propagate in this stage as shown in Figure 2.3 (c) and 2.4 (c). Pores grow perpendicular due to repulsive forces of neighboring pores. Hexagonal arrays of pores are developed in the presence of tensile and compressive stresses because hexagonal shape arrays are favorable in order to minimize the energy of pore formation. Some pores continue to grow while some merge with other as shown in Figure 2.5. Pores are breaking barrier layer and growing into channels, and steady state growth of pores as shown in Figure 2.3 (d) and 2.4 (d) is achieved in this stage [54].

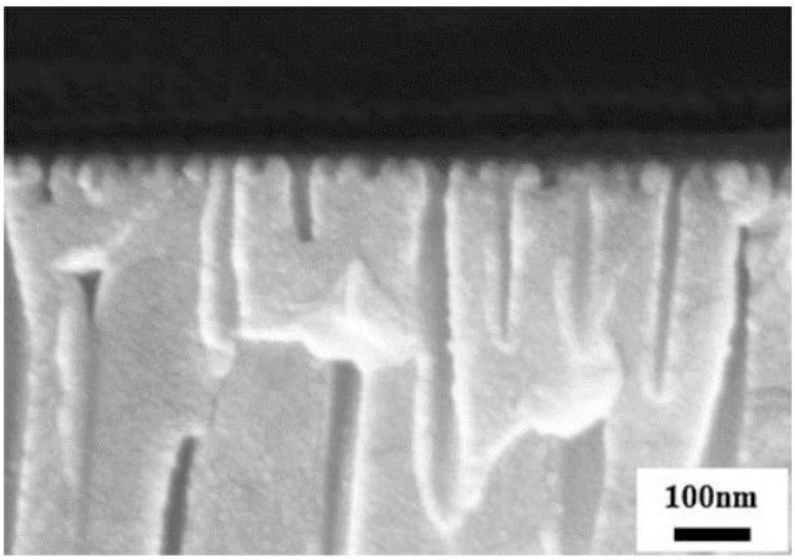

Figure 2.5. Initial pore formation process [55].

2.1.4 Stage d: pore growth

The pores will grow as shown in Figure 2.5, from the confined cracking of the pre formed oxide barrier layers due to internal stresses. The pores are ready to propagate and will grow steadily in equilibrium state. A dynamic equilibrium is achieved by formation and dissolution of anodic aluminum oxide at the same time [56].

2.2 Electrochemical parameters

2.2.1 Electrolyte

Most commonly used electrolytes are sulfuric acid , oxalic axcid, and phosphoric acid yet some also tried selenic acid [57], malonic acid [58], tartaric acid [59], phosphonic acid [60] and etidronic acid [31, 61]. The electrolytes are selected according to the desired pore size of AAO channel. The graphical representation of electrolyte, pore diameter, and voltage is shown in Figure 2.6. In this research work phosphoric acid is used in the range of 60-195 V.

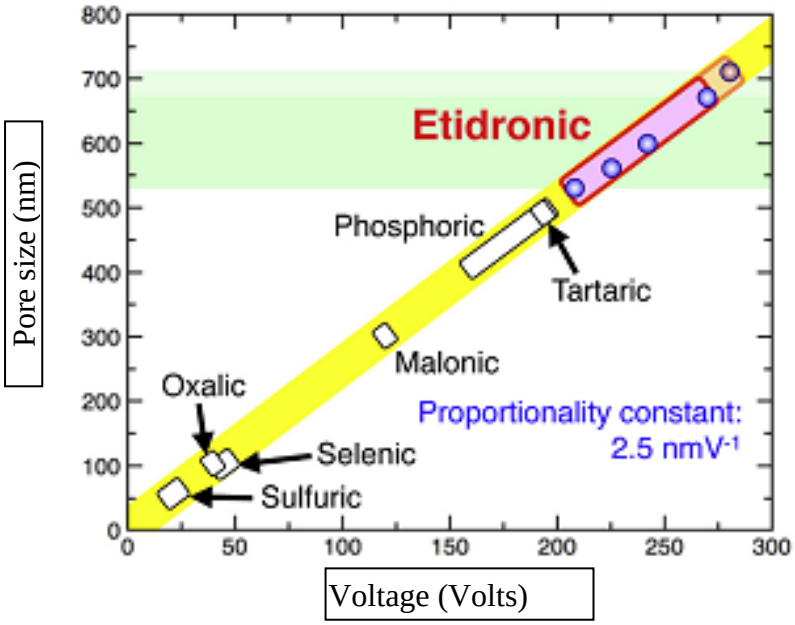

Figure 2.6. Relationship between electrolyte, voltage and pore size [31].

2.2.2 DC voltage

Dc voltage is applied in accordance with electrolyte and required pore size. The general relation between voltage and pore size is as follow:

Pore size = λ * voltage

λ is a process dependent constant which have values in the range of 1.2 to 1.8. By considering λ = 1.5, we have to apply 200 volts to get 300 nm pore size of AAO channels. To increase pore size there are pore widening techniques [62] in which sample is dipped in 5 vol % H_3PO_4 for 30 minutes after first anodization and it can also be increased by two-step anodization

[22, 63] process. Recommended values of voltage against electrolyte are summarized below in Table 2.1.

Electrolyte	Concentration	Voltage	References
Sulfuric Acid H_2SO_4	0.3 M	12V-25 V	[20, 24]
Oxalic Acid $(COOH)_2$	0.3M	30V-60 V	[64-68]
Phosphoric Acid H_3PO_4	0.1 M	90V-195 V	[14, 16, 65, 69]

Table 2.1. Relationship between electrolyte and voltage.

2.2.3 Pore size

Pore size is the key factor in anodization. The combination of anodization paramters are adjusted according to the requirement of final pore size of AAO channels.The pore size is directly proportional to applied voltage irrespective of the substrate [70]. Following is the gist of combination of anodization parameters used by researchers in order to obtain AAO channels.

Electrolyte	**Concentration**	**Voltage (V)**	**Pore Size (nm)**	**Time (hours)**	**References**
Oxalic acid	0.3M	30	40	8,10	[71]
	0.3M	60	80	3,8	[72]
	0.4M	40	50	8,10	[71]
	0.5M	50	80	8,10	[73]
Sulfuric acid	0.5M	18	70	4, variable	[74]
Phosphoric acid	Not Specified	195	200	variable	[75]
	0.4	5 to 40	20 to 75	1 step / variable	[76]

Table 2.2. Voltage, time and final pore size achieved from three commonly used electrolytes for the fabrication of anodic aluminum oxide channels [77].

2.3 Overview of applications

The Figure 2.7 is showing extensive use of anodic aluminum oxide channels in almost every field of science. In biomedical AAO channels are being used for implants, drug delivery, and cell growth. While in electronics, they are used for optical, photonics, magnetism, energy storage, fuel cells and as solar cells. AAO channels are widely used as separation membranes to filter and transport different liquids. Very limited work is done in bio sensing and chemical sensing [78]. Researchers are working on bio sensing by using AAO channels, which will bridge the gap between science and technology. By seeing diversified applications in all fields, there is room to explore its usability in the field of sensing through biological and chemical molecules, which is also a motivation to this research work.

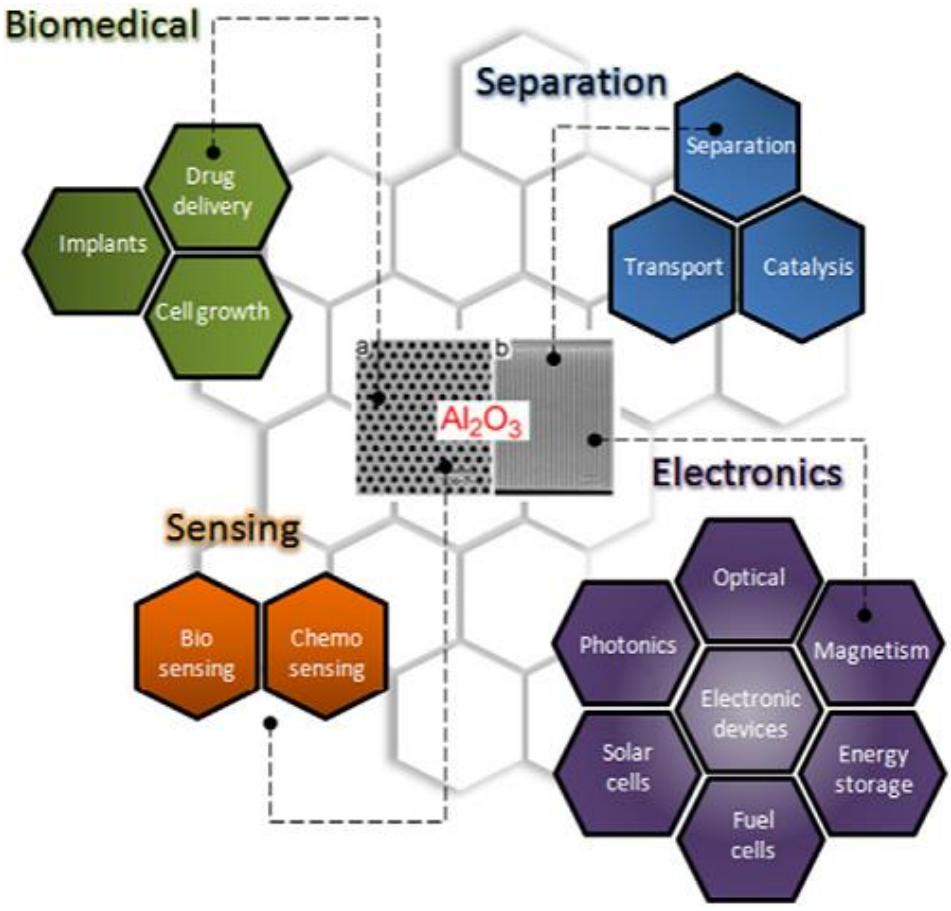

Figure 2.7. A schematic overview of applications of anodic aluminum oxide channels [79].

Chapter 3

Experimental Procedure

3.1. Electrochemical anodization setup

The electrochemical setup is used mostly for fabrication of anodic aluminum oxide channels. The essential part of anodizing setup is DC power supply that should be able to give constant voltage up to 60 V in case of sulfuric and oxalic acid, while 190 DC volts are required for large pore size anodization, which is mostly, performed in phosphoric acid. The remaining accessories are attached according to the final application of anodic aluminum oxide channels. The additional components are digital multimeter, re-circulation chillers for low temperature experiments, inert electrodes, thermometers and mechanical/magnetic stirrers. A computer interface is optional in order to record current output values against applied voltage with respect to time. The current versus time graph obtained from computer interface can help to predict and improve growth of pores. A magnetic stirrer is necessary for high voltage anodization (performed above 60 V) to remove the heat produced on the surface of anode. Components required for electrochemical anodization setup are described here as follows:

3.1.1 Power supply

QPX 1200S power supply as shown in Figure 3.1 was used for anodization experiments performed in the range of 40-60 V while locally manufactured power supply was used for the high voltage anodization experiments up to 190 V.

Figure 3.1. DC Power supply for anodization.

3.1.2 Digital multi-meter

Digital multimeter of Uni-Trend group as shown in Figure 3.2 was used to determine the current vs time behavior. The model used was Uni-T 60-A which had the RS232C interface accessory. The data points are continuously saved in a computer, which are used to generate current profiles. The range (400mA - 10A) of UNI-T 60A was used for anodization experiments.

Figure 3.2. Digital multi-meter.

3.1.3 Computer interface

Digital multi-meter with RS232C as shown in Figure 3.3 is a vital tool to increase the reliability of anodization experiments. The computer interface allows the user to monitor the current vs time readings and help to understand the behavior of pores. The complete growth of pores depends upon the four stages of current vs time graph as explained in section 2.1.

Figure 3.3. Digital multi-meter with computer interface.

3.1.4 Magnetic stirrer

To prevent the localized heating at surface of sample, magnetic stirring is necessary in anodization bath. For this purpose, digital hotplate MSH20D wise stir ® as shown in Figure 3.4 was used for stirring to reduce the heat produced at surface of anode. Stirring can be achieved by mechanical means, or by magnetic means.

Figure 3.4. Digital hotplate and magnetic stirrer.

3.1.5 Re-circulating chiller

A re-circulating chiller of Haake F3 as shown in Figure 3.5 was used to circulate anti-freezing pure iso-propanol to maintain low working temperatures in anodization bath. 1-liter glass beaker was used as an anodization cell that was placed in 2-liter beaker to achieve low working temperatures by means of circulation of pure iso-propanol as shown in Figure 3.5. The anti-freezing solution (pure iso-propanol) enters the 2-liter beaker at inlet, and leave the beaker at outlet as shown in Figure 3.5. The inlet and outlet are connected to re-circulating chiller and its temperature was set to -15^{o}C. The temperature of electrolyte was monitored continuously with the help of thermometers. It was observed that electrolyte temperature in anodization bath is -8^{o}C when re-circulating chiller is set to -15^{o}C.

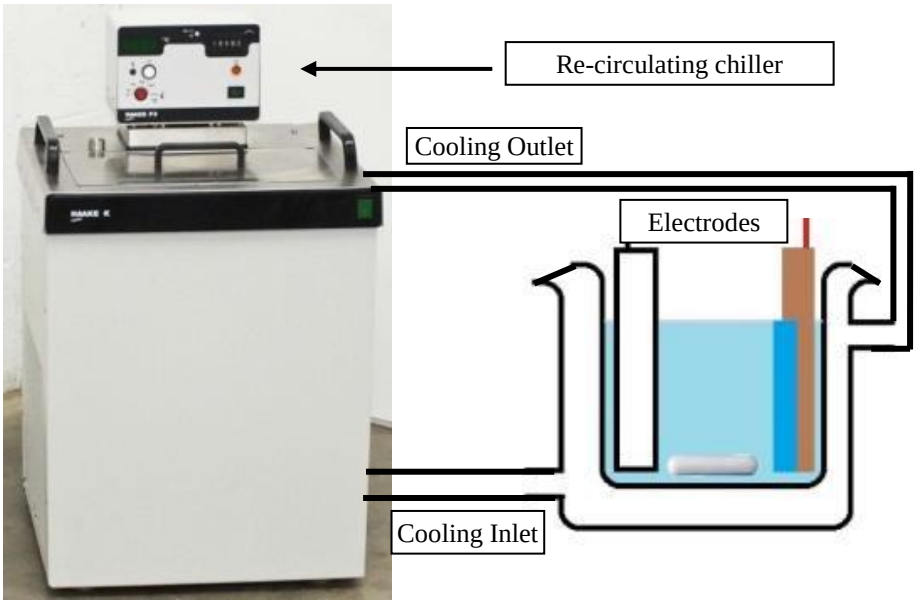

Figure 3.5. Schematic for recirculation of anti-freezing iso-propanol for high voltage experimentation.

3.1.6 Anode

Anode is working electrode in electrochemical anodization. A strip of 1.5 cm long x 4cm wide aluminum foil is used as an anode for all experiments.

3.1.7 Cathode

Cathode can be any inert electrode such as lead, platinum and graphite. Lead is used as inert electrode for all experiments.

3.1.8 Electrolyte

Electrolyte is the solution in which anodization take place; it provides the negative ions to the positive anode. 0.3 M oxalic acid and 5 vol % phosphoric acid was used for all anodization experiments. The preparation of electrolytes for desired concentration is as follows:

a. *0.3 M oxalic acid*

Oxalic acid of analytical grade BDH was used in initial anodization experiments and in first two set of experiments. Oxalic acid is very useful in obtaining regular pores at room temperature [20]. In order to prepare 0.3 molar oxalic acid, 37.821g of dihydrate oxalic acid was added in 1-liter de-ionized water.

b. *5 Vol % Phosphoric acid*

Phosphoric acid is widely used for large pore size anodization. 5 vol % phosphoric acid was used for experiments performed in the range of 60-190 V. It was prepared by adding 50 ml of phosphoric acid into 1-liter de-ionized water.

3.2 Experimental steps

3.2.1 Sample preparation

Sample preparation is very important to obtain high quality AAO channels. First step is to anneal the aluminum foil at 500^{o}C for 5 hours in muffle furnace which help to reduce internal stresses, burning and cracks on the surface of anodized aluminum oxide [52].

3.2.2 Electro polishing

After annealing, samples are electro polished in 2 wt % NaOH and cleaned by rinsing with ethanol.

3.2.3 1st Anodization

In 40-50 V were used as anodizing voltage for 0.3 M oxalic acid while 60-150 V were applied to 5 vol % phosphoric acid for one hour for all samples.

3.2.4 Pore widening

Pore widening is performed after 1st anodization to increase pore size of AAO channels by dipping samples in 5 vol % phosphoric acid at 20^{o}C for 30 minutes for all samples.

3.2.5 2nd anodization

In second anodization, 40-50 V were used as anodizing voltage for 0.3 M oxalic acid while 60-190 V were applied to 5 vol % phosphoric acid for 2-3 hours for all samples.

3.3 Detailed experimental scheme

To optimize the anodization parameters for large pore size AAO channels, preliminary combinations of experiments were performed to obtain regular network of anodic aluminum oxide channels. After successful initial experiments, the anodization setup was designed for low working

temperatures and following set of experiments, as enlisted in Table 3.1, were designed to optimize the anodic aluminum oxide channels on aluminum foil.

S. No	Sample ID	Electrolyte	Time (h)		Temp. (^{o}C)	DC Voltage (V)
			1st A	2nd A		
1.	AO1a	0.3 M Oxalic acid	1	2	5	40
2.	AO1b					
3.	AO1c					
4.	AO2a	0.3 M Oxalic acid	1	2	5	50
5.	AO2b					
6.	AO2c					
7.	AP3a	5 Vol % Phosphoric acid	1	2	-2	60
8.	AP3b					
9.	AP3c					
10.	AP4a	5 Vol % Phosphoric acid	1	Nil	-2	90
11.	AP4b					
12.	AP4c					
13.	AP5a	5 Vol % Phosphoric acid	1	2	-5	110
14.	AP5b					
15.	AP5c					
16.	AP6a	5 Vol % Phosphoric acid	1	2	-5	130
17.	AP6b					
18.	AP6c					
19.	AP7a	5 Vol % Phosphoric acid	1	1.5	-8	150
20.	AP7b					
21.	AP7c					
22.	AP8a	5 Vol % Phosphoric acid	1	2	-8	170
23.	AP8b					
24.	AP8c					
25.	AP9a	5 Vol % Phosphoric acid	1	3	-8	190
26.	AP9b					
27.	AP9c					

Table 3.1. Experimental plan for anodization at different voltages and temperatures.

3.4 Anodization cell

A beaker of 2000 ml was used throughout in experimentation for re-circulation of anti-freezing iso-propanol solution and for holding anodization cell of 1000 ml beaker as shown in Figure 3.6 that has the electrolyte, anode, cathode, magnetic stirring bar and thermometer. Digital ammeter with RS232C cable was connected to computer that records the output current of anodization experiments with respect to time, while digital voltmeter was connected to monitor the voltage values. Thermometer was placed in an anodization cell to observe the temperature of an electrolyte throughout the experimentation. Magnetic stirrer was used in order to minimize the heat generated at surface of sample. The schematic of complete setup is depicted in Figure 3.6.

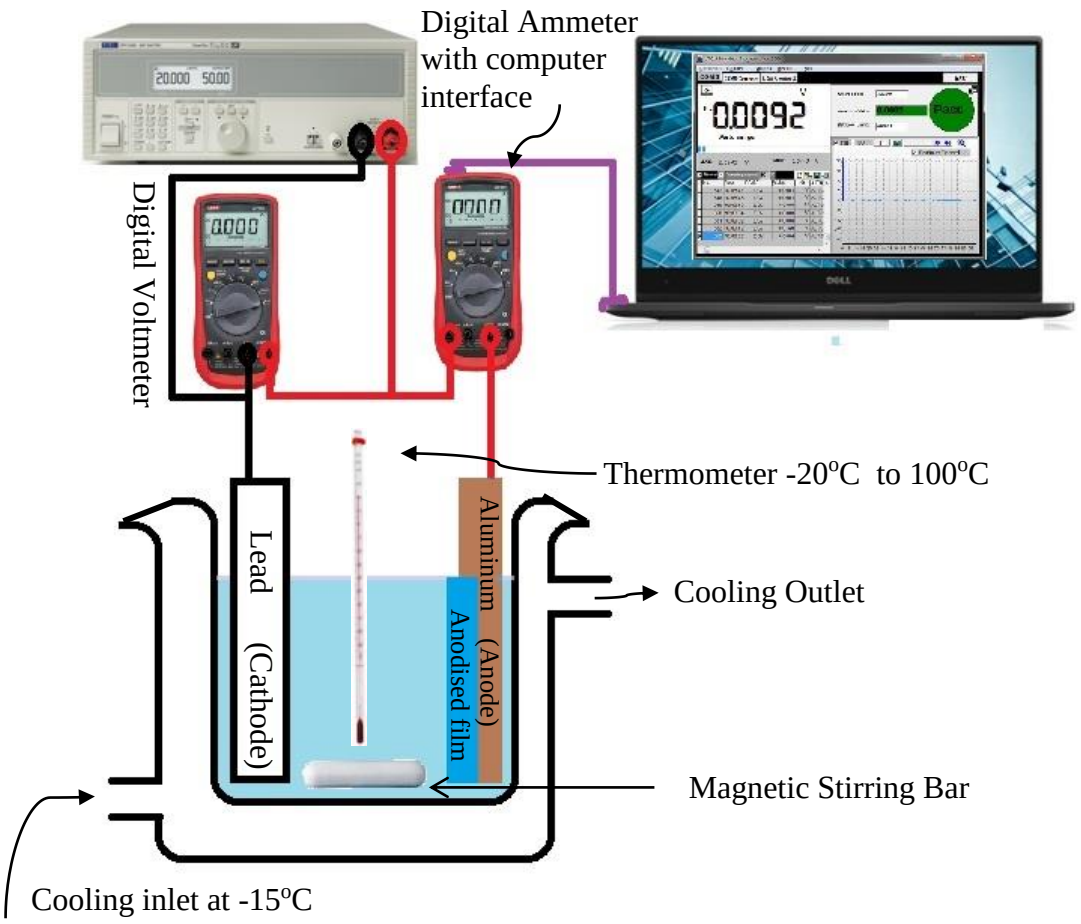

Figure 3.6. Schematic of setup used to fabricate anodic aluminum oxide channels.

Chapter 4

Results and Discussion

4.1 SEM results and current profiles

To optimize anodic aluminum oxide channels, experiments are divided into nine sets based on voltage range of 40-190 V. Following are the results and discussion for each set of experiment.

4.1.1 Surface analysis of AAO obtained at 40 V

Good and continuous porous network is obtained for anodization performed at 40 V in 0.3 M oxalic acid. The parameters for anodization are given in Table 4.1.

Sample	Electrolyte	Time (h)		Temp (^oC)	DC Voltage (V)	Pore Size obtained (nm)
		1st A	2nd A			
AO1	0.3 M Oxalic acid	1	2	5	40	40 ±5

Table 4.1. Parameters for anodization performed at 40 V in 0.3 M oxalic acid.

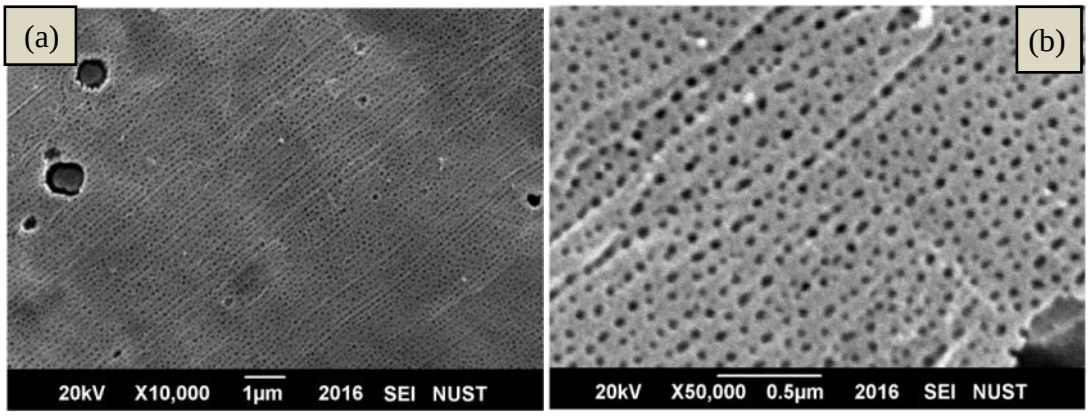

Figure 4.1. SEM micrographs for anodization of aluminum foil performed in 0.3 M oxalic acid at 40 V and 5^{o}C (a) at magnification of 10000x (b) at magnification of 50000x.

Figure 4.1 is showing a good, regular and homogenous network of anodic aluminum oxide pores. There are some cavities present at the surface of aluminum foil due to formation of inter-metallic compounds. These inter-metallic compounds can be minimized by pre-treatments and improving the purity of aluminum foil. The average pore size obtained from this set of experiments is 40 ±5 nm.

4.1.2 Surface analysis of AAO obtained at 50 V

This set of experiment was performed to increase the pore size of anodic aluminum oxide channels from previous set of experiment (section 4.1.1). The anodization voltage was increased to 50 V and other parameters were kept same and given in Table 4.2.

Sample	**Electrolyte**	**Time (h)**		**Temp (°C)**	**DC Voltage (V)**	**Pore Size obtained (nm)**
		1st A	2nd A			
AO2	0.3 M Oxalic acid	1	2	5	50	45 ±4

Table 4.2. Parameters for anodization performed at 50 V in 0.3 M oxalic acid.

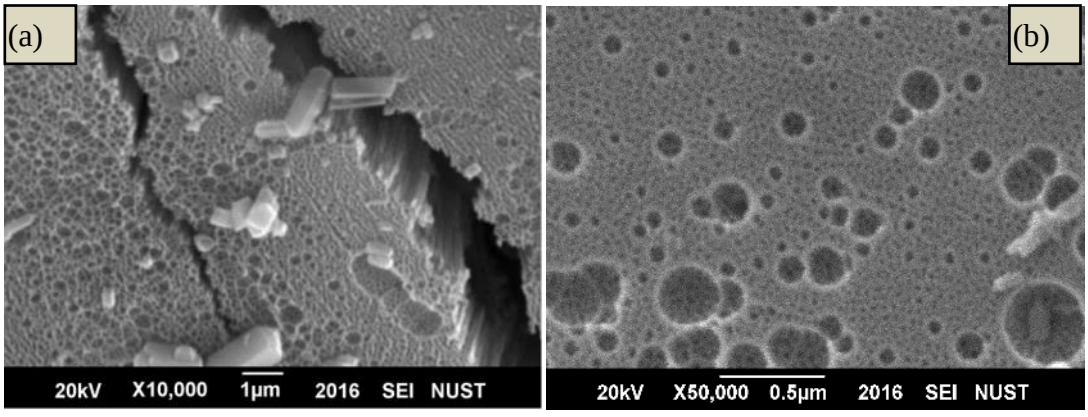

Figure 4.2 SEM micrographs for anodization of aluminum foil performed in 0.3 M oxalic acid at 50 V and 5°C (a) cross sectional view for AAO channels (b) top view of anodized aluminum oxide with bigger pores on surface.

From Figure 4.2. pores are continuous and channels are formed in depth of aluminum foil. Although there are some unnecessary large pores on the surface (see Figure 4.2 (a) mentioned in Figure 4.2) which are due to little variations in electrolyte temperature.

4.1.3 Surface analysis of AAO obtained at 60 V

In this set of experiment, voltage was increased to 60 V and temperature was reduced to 2^{o}C. High voltage anodization produces heat at the surface of sample. In order to overcome the heat generation, temperature was reduced to 2^{o}C. The anodization parameters for this set of experiment are given in Table 4.3.

Sample	Electrolyte	Time (h)		Temp (^{o}C)	DC Voltage (V)	Result
		1st A	2nd A			
AP3 a	5 Vol % Phosphoric Acid	1	2	2	60	Burned
AP3 b				-2		Pores Initiated

Table 4.3. Parameters for anodization performed at 60 V in phosphoric acid.

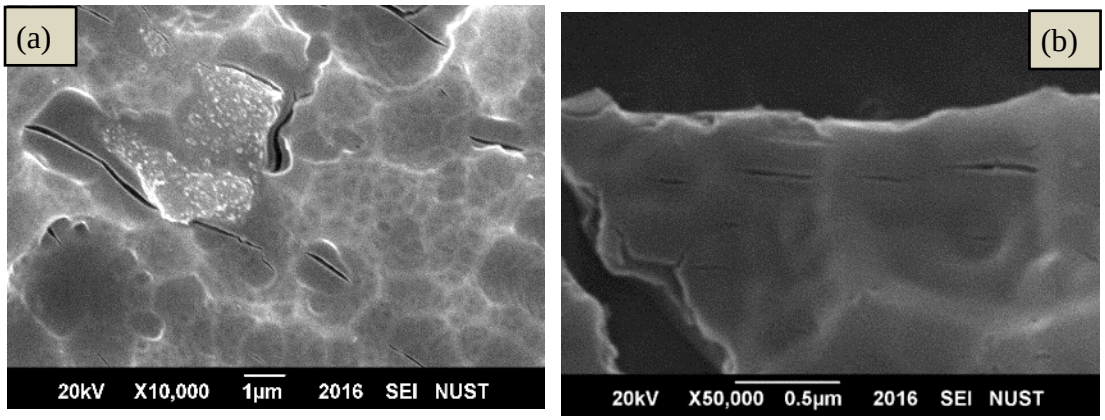

Figure 4.3 SEM micrographs of anodization performed at 60 V in 5 vol % phosphoric acid at 2^{o}C (a) burned sample with cracks (b) one major crack with no pores on surface.

In this set of experiments, samples were not anodized efficiently due to overheating of samples at 60 V. The temperature was not enough to minimize the cracks on the surface of aluminum foil as seen in Figure 4.3. After obtaining burned samples, experiment was improved by reducing temperature to -2^{o}C and by keeping all other parameters same. It was noticed that cracking and burning is reduced as shown in Figure 4.4 by decreasing working temperature.

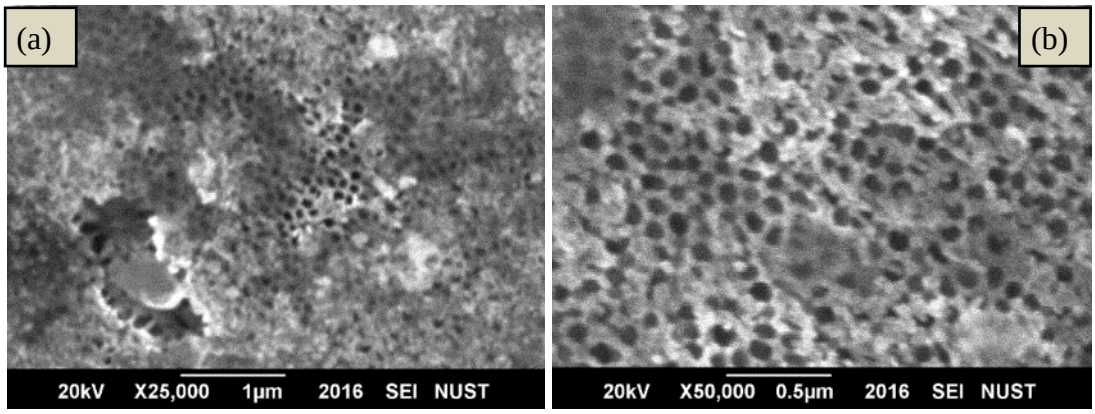

Figure 4.4. SEM micrographs for anodization performed at 60 V in 5 vol % phosphoric acid at -2^{o}C (a) No cracks and burning effects on surface of anodized aluminum foil (b) formation of pores due to reduced working temperature with no visible cracks at higher magnification.

4.1.4 Surface analysis of AAO obtained at 90 V

After successful pore initiation in phosphoric acid at low working temperatures, magnetic stirrer was added in an anodization setup in order to disspate the heat produced from surface of sample to anodization bath. The magnetic stirring of electrolyte helped to get regular and homogenized porous network as shown in Figure 4.5. The samples were anodized according to parameters listed in Table 4.4. SEM was performed as shown in Figure 4.5 after first anodization to observe the stirring effect on the surface of anodized aluminum foil.

Sample	**Electrolyte**	**Time (h)**		**Temp (^{o}C)**	**DC Voltage (V)**	**Pore Size Obtained (nm)**
		1st A	**Pore widening**			
AP4	5 Vol % Phosphoric Acid	1	0.5	-2	90	100 ±18

Table 4.4. Parameters for anodization performed at 90 V in 5 vol % phosphoric acid.

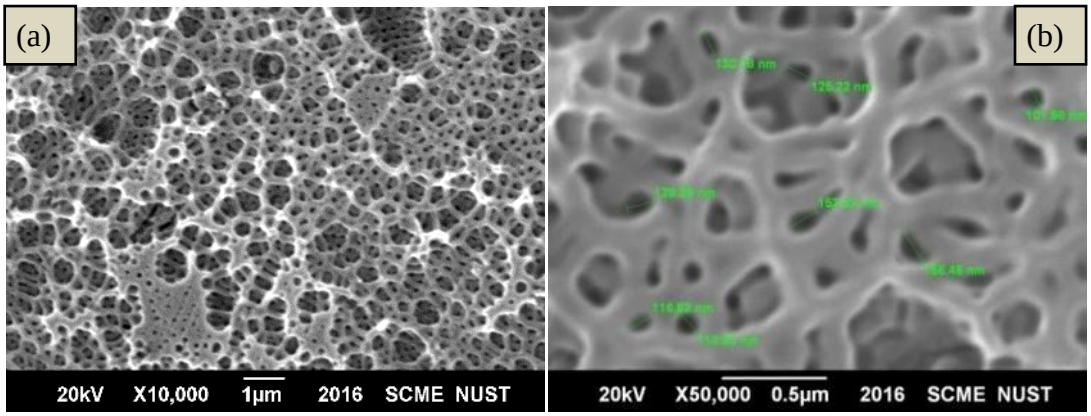

Figure 4.5. SEM micrographs for anodized aluminum foil obtained after first anodization in 5 vol % phosphoric acid at 90 V and -2°C (a) continuous network of pores due to magnetic stirring (b) higher magnification image showing irregular pores on surface of anodized aluminum foil.

4.1.5 Surface analysis of AAO obtained at 110 V

After obtaining regular porous network at 90 V with the help of magnetic stirring, the next goal was to get larger pores by performing anodization at higher voltages. As from previous set of experiments, it was observed that magnetic stirring and low working temperature plays a key role in obtaining homogenous network, so this set of experiment was performed at -5°C along with magnetic stirring. The voltage was increased to 110 V as an intention of getting large size of pores as applied voltage is directly proportional to the final pore size of anodized aluminum oxide channel [31]. Other parameters for this set of experiments are enlisted in Table 4.5.

Sample	**Electrolyte**	**Time (h)**		**Temp (°C)**	**DC Voltage (V)**	**Pore Size obtained (nm)**
		1st A	**2nd A**			
AP5	5 Vol % Phosphoric Acid	1	2	-5	110	160 ±11

Table 4.5. Parameters for anodization performed at 110 V in 5 vol % phosphoric acid.

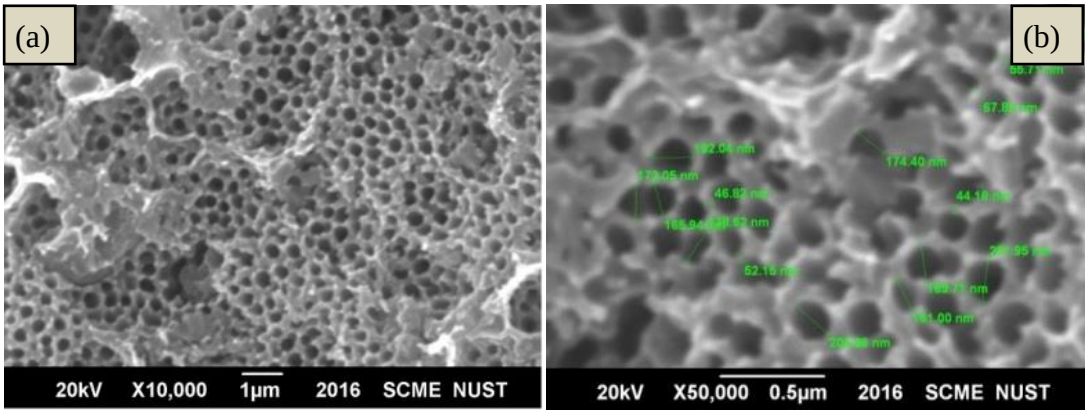

Figure 4.6. SEM micrographs for anodized aluminum foil obtained in 5 vol % phosphoric acid at110 V and -5^{o}C (a) regular and homogenous network of pores on surface of anodized aluminum (b) large size and regular anodic aluminum oxide pores.

From SEM images presented above in Figure 4.6 (a), the regularity and continuity in porous network is achieved by performing anodization at -5^{o}C. The reduced working temperature also helped to control the heat generataion issue at the surface of sample. In Figure 4.6 (b) average pore size is found to be 160 nm. Ther are no signs of burns and cracks at higher voltage anodization due to continuous stirring of electrolyte and because of re-circulating chiller which is maintaining the temperature at -5^{o}C.

4.1.6 Surface and cross sectional analysis of AAO obtained at 130 V

After removing heat effects and obtaing regularity at higher voltage anodization, next set of experiments are focused on increasing the pore size of anodic aluminum oxide channels. This set of experiment was performed according to electrochemical parameters given in Table 4.6.

Sample	Electrolyte	Time (h)		Temp (^{o}C)	DC Voltage (V)	Pore Size Obtained (nm)
		1st A	2nd A			
AP6	5 Vol % Phosphoric Acid	1	2	-5	130	180 ±18

Table 4.6. Parameters for anodization performed at 130 V in 5 vol % phosphoric acid.

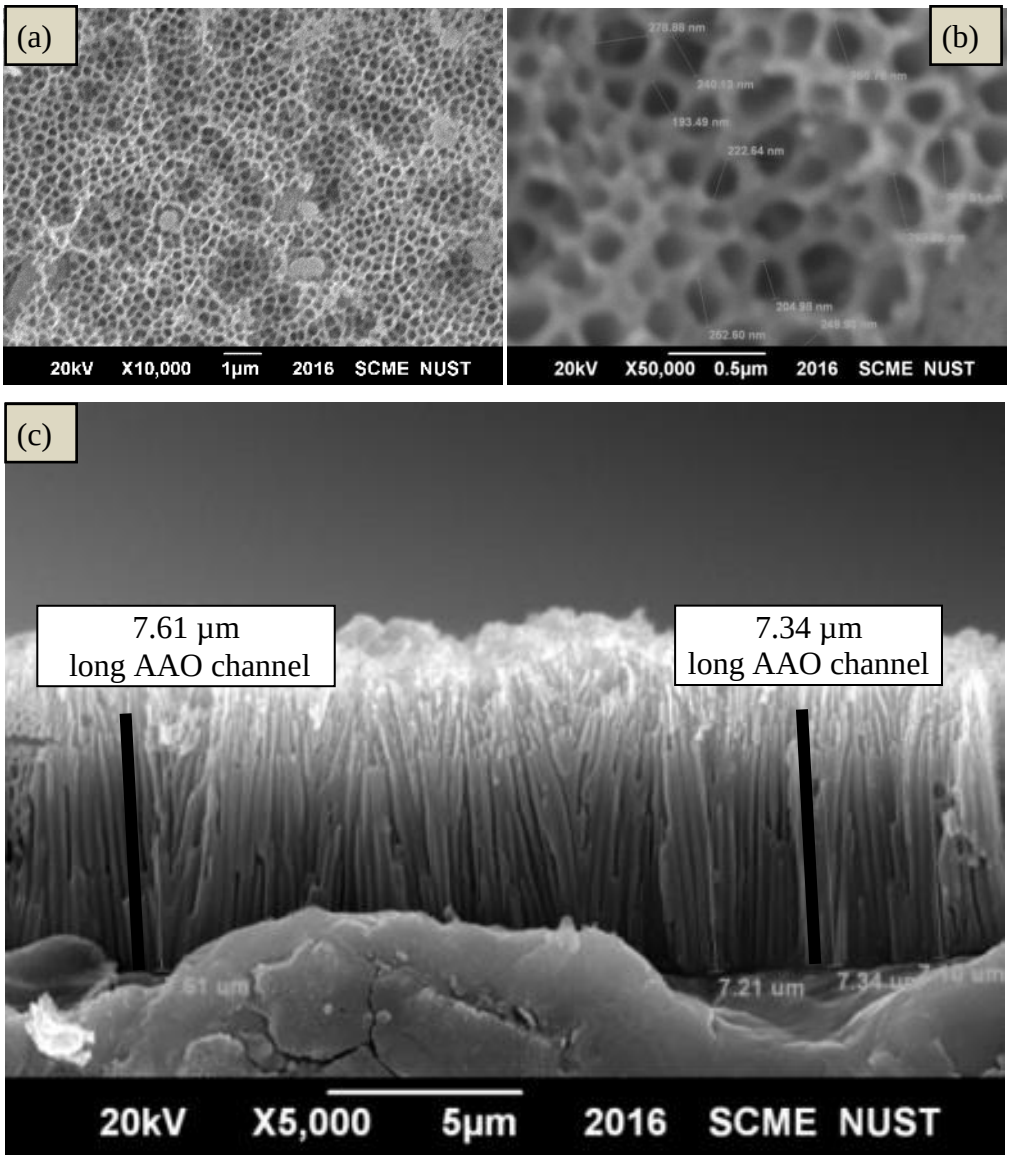

Figure 4.7. SEM micrographs for anodized aluminum foil obtained in 5 vol % phosphoric acid at130 V and -5ºC (a) At lower magnification showing extensive porous structure (b) At higher magnification showing uniform and self-organized network of pores (c) cross section view of anodized aluminum foil to observe AAO channels.

From SEM images shown in Figure 4.7 (a) and (b), pores are regular and self-ordered. Pore size is increased to 180 nm with approximate 7 µm long AAO channels as shown in Figure 4.7 (c). This set of experiment produced best results in terms of pore size and channel length against the applied electrochemical parameters.

4.1.7 Surface and cross sectional analysis of AAO obtained at 150 V

After obtaining self-ordered pores with channels, voltage was increased to 150 V and temperature was decreased to -8^{o}C to increase the pore size at AAO channels. Parameters for this set of experiments are listed in Table 4.7.

Sample	Electrolyte	Time (h)		Temp (^{o}C)	DC Voltage (V)	Pore Size Obtained (nm)
		1st A	2nd A			
AP7	5 Vol % Phosphoric Acid	1	1.5	-8	150	190 ±32

Table 4.7. Parameters for anodization performed at 150 V in 5 vol % phosphoric acid.

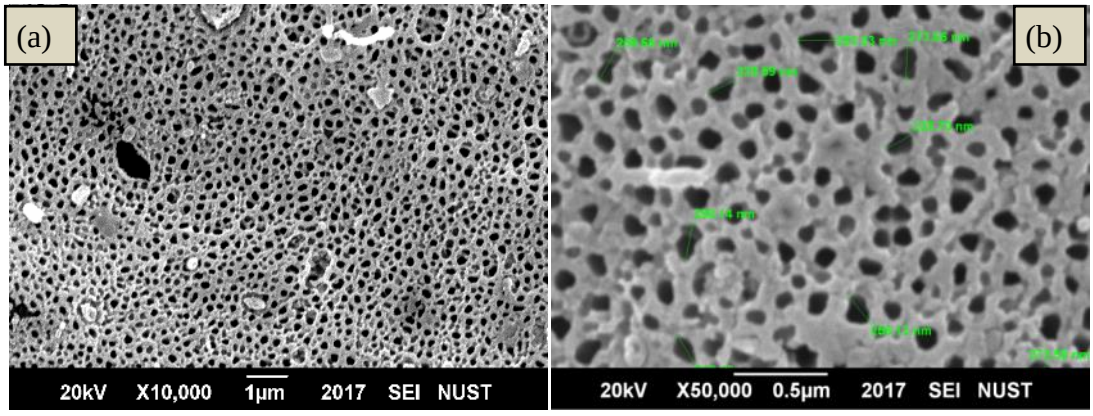

Figure 4.8. SEM micrographs for anodized aluminum foil obtained in 5 vol % phosphoric acid at 150 V and -8^{o}C (a) uniform and continuous porous network with few cavities (b) porous network at higher magnification to observe cracks and irregularities on surface of anodized aluminum foil.

From SEM images of AAO channels, (Figure 4.8 (a) and (b)) this set of experiment produced better results regarding heat effects as working temperature reduced to -8^{o}C. At low magnification, there is one large cavity present in Figure 4.8 (a) which is due to an impurity present in aluminum foil. The impurities react with acidic electrolyte and leave the cavity on the surface of sample [80]. The average pore size obtained from this set of experiments is 190 ±32nm.

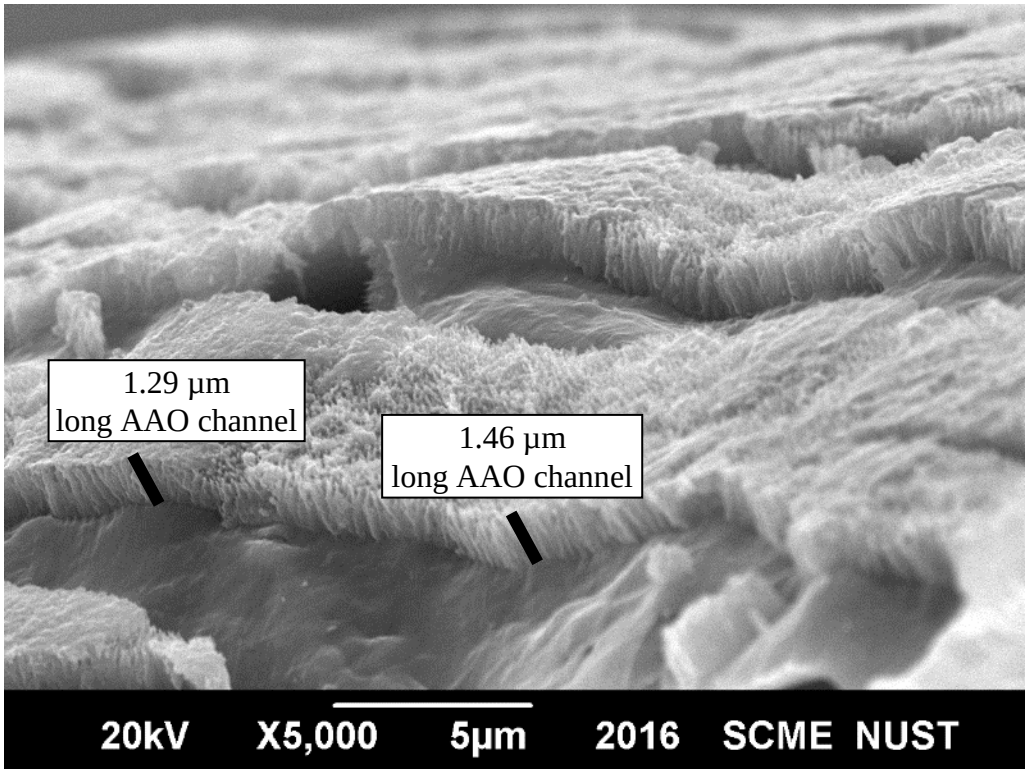

Figure 4.9. SEM image for cross section view of anodized aluminum oxide obtained in 5 vol % phosphoric acid at 150 V and -8ºC.

Figure 4.9 is showing colonies of AAO channels with top surface and cross sectional view of anodized aluminum foil. The AAO channels in this set of experiment are short as compared to previous set of experiment. The reason for short length of channels is that second anodization is performed for short time because of inter-metallic compounds. When inter-metallic compounds are formed, they left a cavity on the surface [80] which increase the current density in that region and in turn more heat is generated at the surface of sample which disrupts the overall working temperature.

4.1.8 Surface and cross sectional analysis of AAO obtained at 170 V

After achieving self-ordered and regular pores in previous experiments, this set of experiment was performed in order to increase pore size by increasing applied voltage. The length of channels depends on the time given to second anodization, so in this set of experiment, second anodization was performed for 30 minutes more than previous set of experiment. The parameters used for anodization at 170 V are given in Table 4.8:

Sample	Electrolyte	Time (h)		Temp (°C)	DC Voltage (V)	Pore Size Obtained (nm)
		1st A	2nd A			
AP8	5 Vol % Phosphoric Acid	1	2	-8	170	220 ±20

Table 4.8. Parameters for anodization performed at 170 V in 5 vol % phosphoric acid.

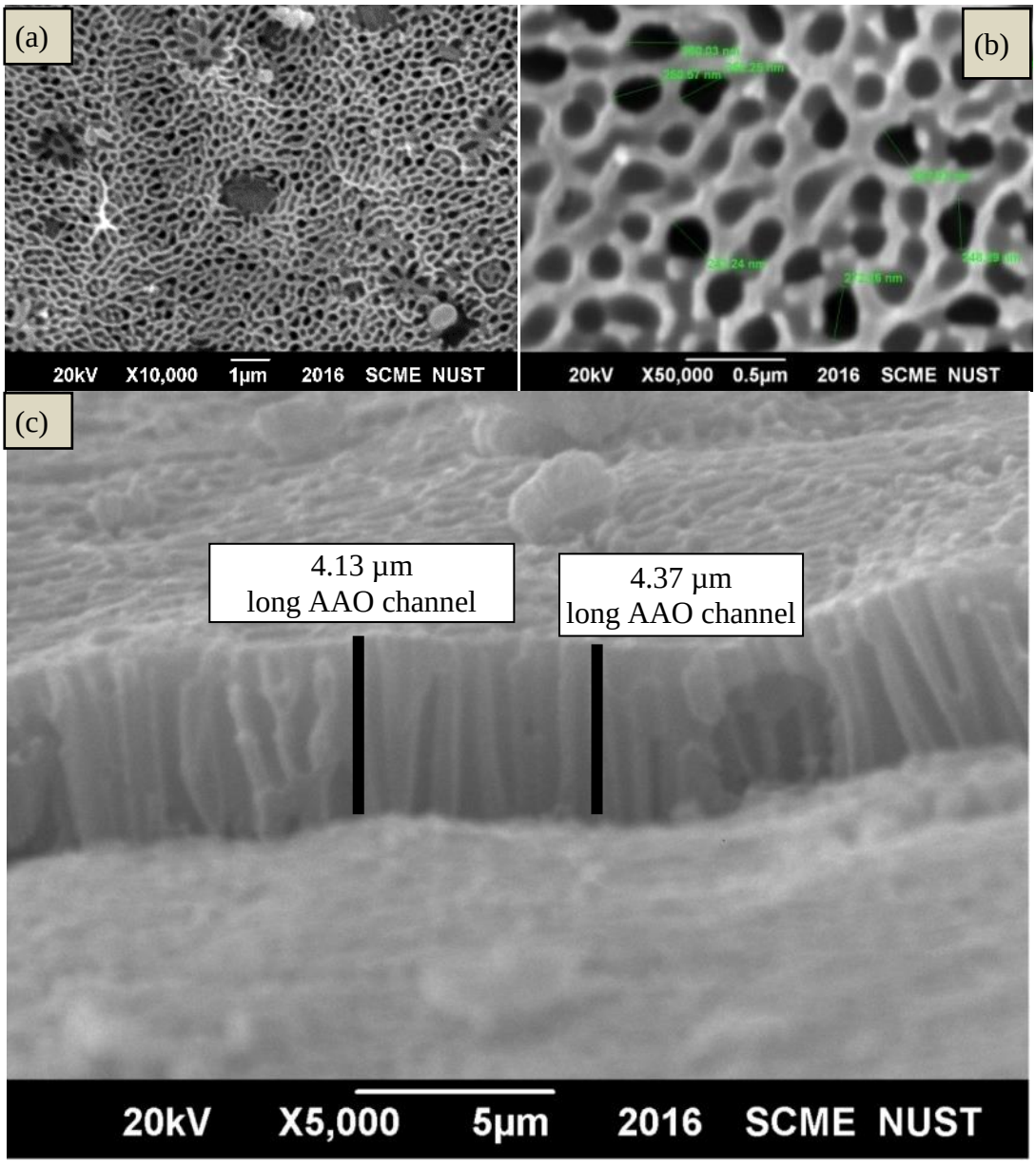

Figure 4.10. SEM micrographs for anodized aluminum foil obtained in 5 vol % phosphoric acid at170 V and -8°C (a) At lower magnification showing homogenous porous structure (b) At higher magnification showing morphology of pores (c) Cross section view of channels along with pores on surface.

From SEM images Figure 4.10 (a) and (b) it is observed that pores are continuous and regular in geometry. In this set of experiment, there are no cracks, burning and local heating effects on the surface of sample. The average pore size obtained at surface of anodized aluminum foil is 220 ±20 nm. The channels along with pores at surface of aluminum foil as shown in Figure 4.10 (c) are 4 µm long. As the time given in this set of experiment is more during second anodization, so AAO channels also attain more length than anodization performed at 150 V.

4.1.9 Surface and cross sectional analysis of AAO obtained at 190 V

By previous eight set of experiments, the electrochemical parameters are optimized to get large size pores by anodization on aluminum foil. This is the final set of experiment for optimization of AAO channels in which temperature was maintained at -8^{o}C and voltage was increased to 190. The parameters for this set of experiments are listed in Table 4.9.

Sample	Electrolyte	Time (h)		Temp (^{o}C)	DC Voltage (V)	Pore Size Obtained (nm)
		1st A	2nd A			
AP9	5 Vol % Phosphoric Acid	1	3	-8	190	270 ±13

Table 4.9. Parameters for anodization performed at 190 V in 5 vol % phosphoric acid.

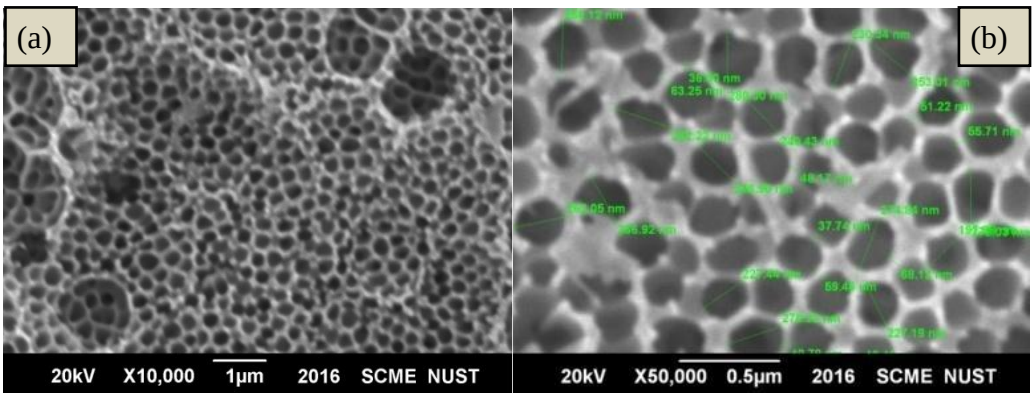

Figure 4.11. SEM micrographs for anodized aluminum foil obtained in 5 vol % phosphoric acid at190 V and -8^{o}C (a) At lower magnification showing self-ordered porous structure (b) At higher magnification showing hexagonal arrays.

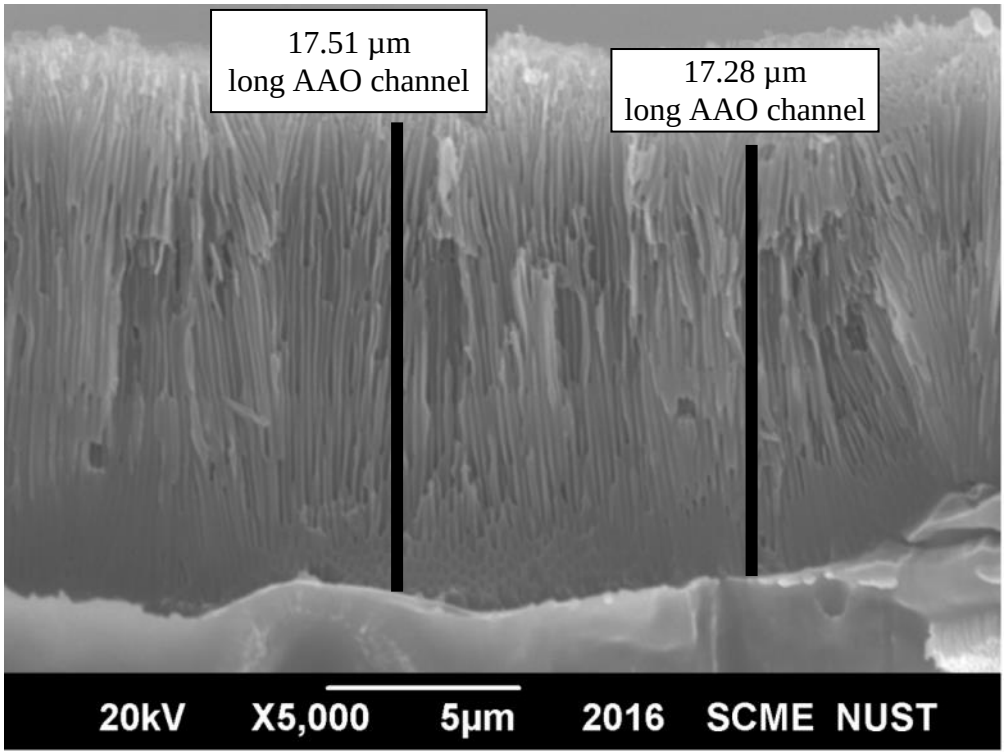

Figure 4.12. Cross sectional view of anodized aluminum foil obtained in 5 vol % phosphoric acid at 190 V and -8ºC showing 17 µm long AAO channels.

In Figure 4.11 (a) a regular self-ordered hexagonal porous network of anodic aluminum oxide channels is seen and in Figure 4.11 (b) it is magnified to measure the pore size with good precision. The pore size is found to be around 270 nm with standard deviation of 13 nm. To get the cross section of aluminum foil, the sample attached in perpendicular direction in SEM sample chamber to observe the channels. The channels length is 17µm as shown in Figure 4.12.

4.2 Comparison of current profiles

The current profiles are function of current and time that give the predictive knowledge of pore formation. In start, the current increase due to resistance of barrier layer and then after breaching barrier layer, it starts to decrease as shown in Figure 4.13. Afterwards it achieves steady state and anodization is performed for required time.

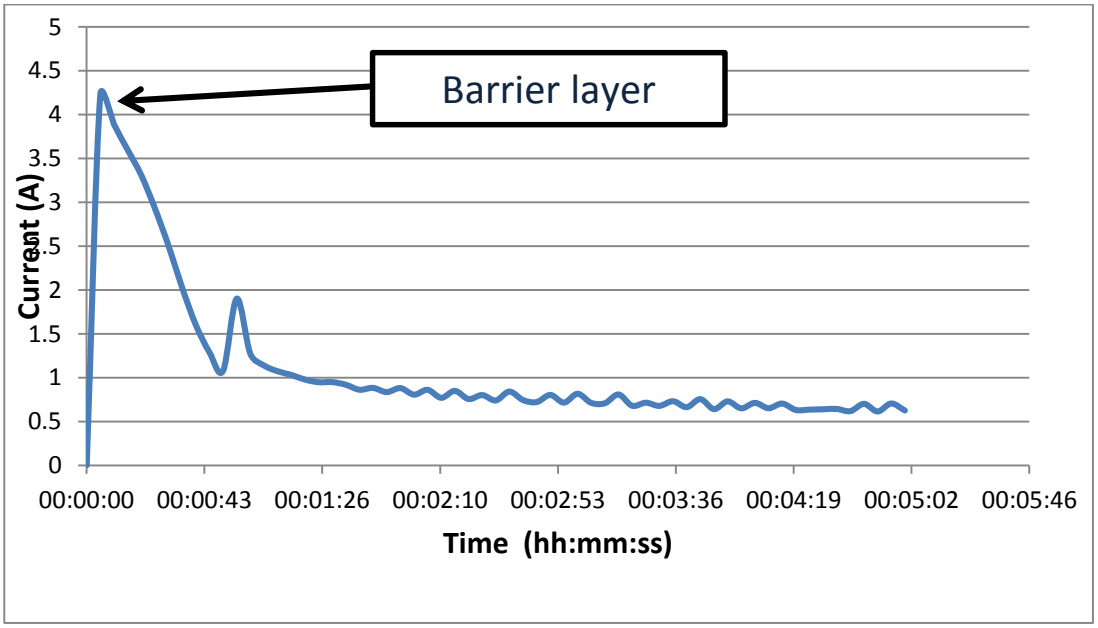

Figure 4.13. Initial current profile of anodization of aluminum foil.

In Figure 4.14, the curve is showing abrupt increase in current values at final stage. This abrupt change is linked with burning and cracking of samples as shown in Figure 4.3 on page 27. These cracks and burns are produced due to heat generated at surface of sample and can be reduced by magnetic stirring and low working temperatures. All remaining samples have similar current profile as shown in Figure 4.14.

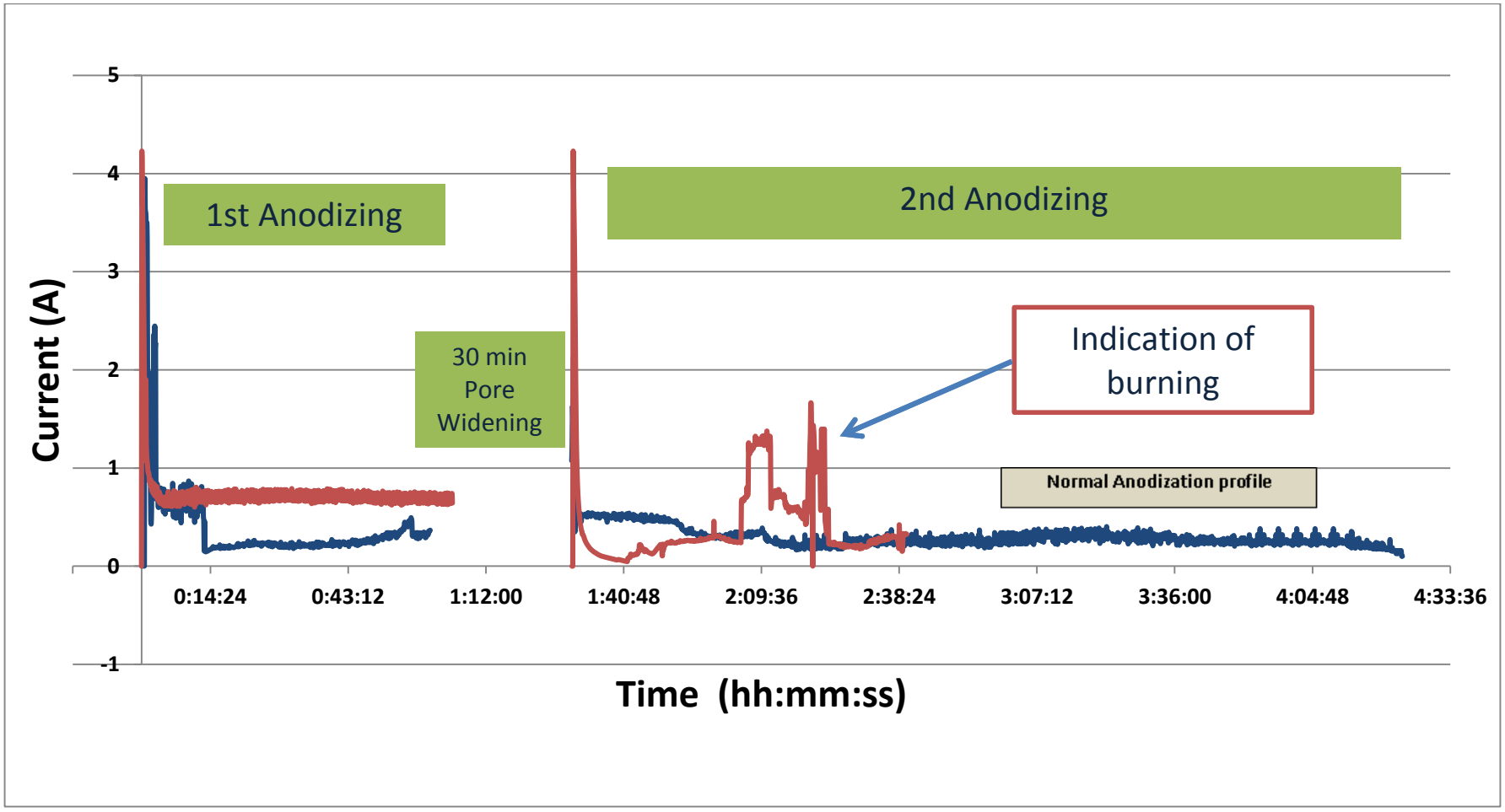

Figure 4.14. Comparison of current profiles for burned and normal samples after anodization of aluminum foil.

4.3 LC alignment on commercial anodisc ® AAO channels

4.3.1 SEM of anodisc ® AAO channles

SEM of anodisc ® aluminum oxide channels was performed as shown in Figure 4.15. The average pore size observed from SEM is 94.5 nm.

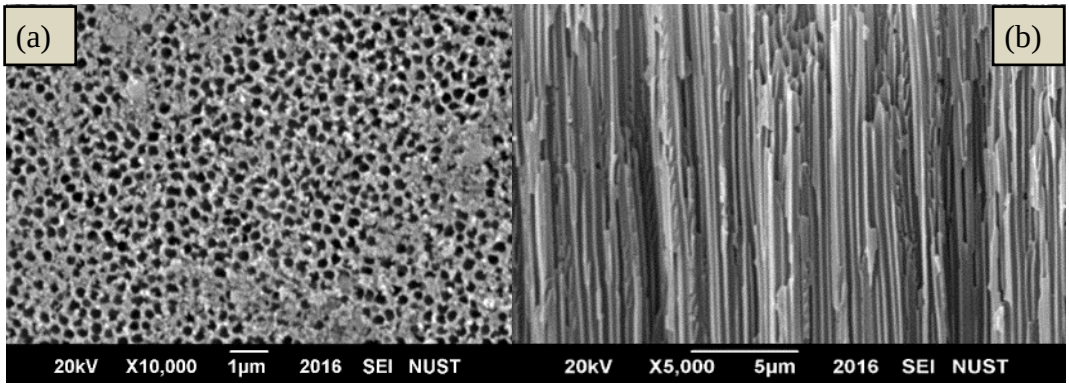

Figure 4.15. SEM micrographs of commercially available anodisc ® AAO channels (a) Top surface view for average pore size and morphology (b) cross sectional view for channels.

4.3.2 LC alignment on anodisc ® AAO channels

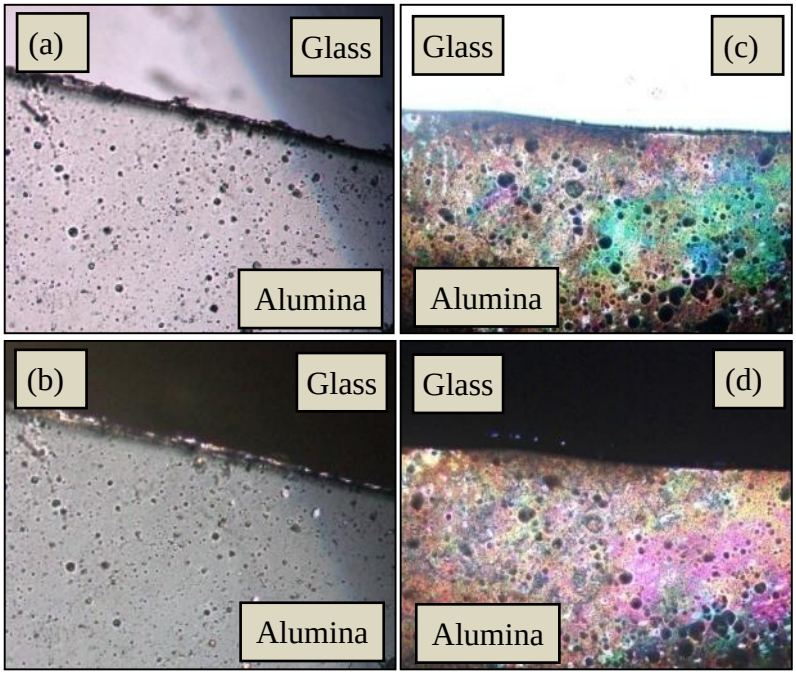

Figure 4.16. Observation of light transmittance under optical microscope for LC alignment in anodisc ® AAO channels (a) bright field image before annealing (b) dark field image before annealing (c) light is blocked due to perpendicular alignment of LC molecules after annealing (d) light is blocked through glass and AAO channels due to perpendicular alignment of LC molecules after annealing.

Liquid crystal alignment on commercially available anodisc ® AAO channels is carried out by attaching it on glass slide with the help of transparent adhesive tape. A small quantity of LC was applied on these channels and optical microscopy was performed as shown in Figure 4.16. AAO channels were observed before and after annealing of LC molecules. When LC molecules are annealed, they are transformed from smectic phase (random orientation) to nematic phase (perpendicular orientation). Figure 4.16 (a) is showing that LC molecules are confined in AAO channels and partial light is allowed due to random orientation of LC molecules. In Figure 4.16 (b) AAO channels are observed under dark field in which light is blocked by glass slide. In Figure 4.16 (c) AAO channels are observed after annealing under bright field in which LC molecules are not transmitting light due to perpendicular alignment of LC molecules. This is further confirmed from Figure 4.16 (d) by observing AAO channels under dark field when light is blocked by applying cross polarizer. By observing AAO channels before and after annealing of LC molecules under polarized optical microscope, it is concluded that LC molecules are confined and perpendicular alignment is achieved in these commercially available anodisc ® AAO channels.

4.4 Comparison of research work

This research work is carried out on 25 µm thin aluminum foil anodized at 190 V in phosphoric acid that resulted in 270 nm pore size of AAO channels, while many researchers perform high voltage anodization on samples having thickness more than 100 µm. Chowdhury et al. [3] used 130-500 µm thick aluminum foil and obtained 80 nm pore size at surface of AAO channels at 60 V in phosphoric acid. Moreover the anodization performed at high voltage effect the surface by burning of AAO channels as reported by Montero et al. [66] yet in this research work burning is successfully avoided at high voltage anodization as shown in Figure 4.11 on page 34. The anodization of impure aluminum foil results in poor morphology and ordering of AAO channels as presented in Figure 4.17 (a) performed by Budiman et al. [81] is showing poor ordering while in this research work, an impure aluminum foil is used for optimization of anodic aluminum oxide

channels through anodization that resulted in continuous, self-ordered and homogeneous porous network as shown in Figure 4.17 (b).

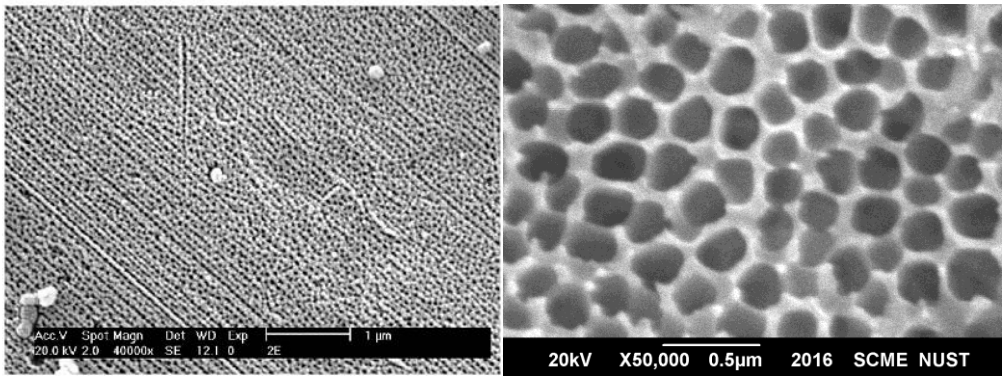

Figure 4.17. SEM micrographs of AAO channels obtained through anodization on (a) impure aluminum foil anodized by Budiman et al. [81] (b) impure aluminum foil anodized in this research work.

4.5 Future perspective

Considering the results presented in this thesis, the key points on the fabrication of anodic aluminum oxide channels have been identified. However, little variation in anodization parameters can be made to obtain through holes and close-ended pores, depending on the intended applications. To move forward in the exploitation of anodic aluminum oxide applications, following directions are suggested for the new researchers:

- Anodization of pure and thin aluminum coated on glass slides to test for liquid crystal based sensing applications.

- Preparation of anodized membranes of desired pore size on thin films for nano-filtration.

Conclusions

1. AAO channels are successfully fabricated by controlling different set of electrochemical parameters through anodization on impure aluminum foil.

2. Annealing and pre-treatments of impure aluminum foils prior to anodization, increase the regularity and surface morphology of AAO channels.

3. For aluminum samples, low working temperature of electrolyte in the range of -2 to -8^{o}C is very essential to compensate the local heat generated at the surface during anodization.

4. Continuous stirring of electrolyte maintains the overall temperature of anodization cell and it improves the hexagonal ordering and continuity of porous network of AAO channels.

5. Lower anodizing voltage will yield smaller pores as anodization performed in oxalic acid at 40 V produced 40 nm pores of aluminum oxide while anodization performed in phosphoric acid at 190 V produced 270 nm pores of AAO channels.

6. AAO channels are successfully optimized at different set of experiments for pore size ranging from 40-270 nm with 1-17 um long channels through anodization on impure aluminum foil.

References

[1] Wang X., Han, Gao-Rong, *Fabrication and characterization of anodic aluminum oxide template.* Microelectronic Engineering, 2003. **66**(4): p. 166-170.

[2] Keller F., Hunter S., Robinson L., *Structural Features of Oxide Coatings on Aluminum.* Journal of The Electrochemical Society, 1953. **100**(9):p. 411-419.

[3] Chowdhury P, Krishnan M, Barshilia, Harish C, Rajam S., *Effect of process parameters on growth rate and diameter of nano-porous alumina templates.* Bulletin of Materials Science, 2011. **34**(3): p. 423-427.

[4] Masuda H., Fukuda K., *Ordered metal nanohole arrays made by a two-step replication of honeycomb structures of anodic alumina.* Science, 1995. **268**(5216): p. 1466-8.

[5] Jeong C., Lee J., Sheppard K., Choi C. H., *Air-Impregnated Nanoporous Anodic Aluminum Oxide Layers for Enhancing the Corrosion Resistance of Aluminum.* Journal of surfaces and colloids, 2015. **31**(40): p. 11040-50.

[6] Shaffei F., Abd El-Rehim, Shaaban A., Huisen S., *Electrolytic coloring of anodic aluminum for selective solar absorbing films: use of additives promoting color depth and rate.* Renewable Energy, 2001. **23**(3-4): p. 489-495.

[7] Andersson, Hunderi O., Granqvist G., *Nickel pigmented anodic aluminum oxide for selective absorption of solar energy.* Journal of Applied Physics, 1980. **51**(1): p. 754-764.

[8] Liu L., Zhao, Yaomin, Zhou, Qin, Xu, Hong, Zhao, Chongjun, Jiang, Zhiyu, *Nano-polypyrrole supercapacitor arrays prepared by layer-by-layer assembling method in anodic aluminum oxide templates.* Journal of Solid State Electrochemistry, 2005. **11**(1): p. 32-37.

[9] Babakhani B., Ivey, Douglas G., *Anodic deposition of manganese oxide electrodes with rod-like structures for application as electrochemical capacitors.* Journal of Power Sources, 2010. **195**(7): p. 2110-2117.

[10] Belwalkar A., Grasing E., Van Geertruyden W., Huang Z., Misiolek W. Z., *Effect of Processing Parameters on Pore Structure and Thickness of Anodic*

Aluminum Oxide (AAO) Tubular Membranes. Journal of membrane science, 2008. **319**(1-2): p. 192-198.

[11] Jia R.P., Shen Y., Luo H. Q., Chen X. G., Hu Z. D., Xue D. S., *Enhanced photoluminescence properties of morin and trypsin absorbed on porous alumina films with ordered pores array.* Solid State Communications, 2004. **130**(6): p. 367-372.

[12] Santos A., Macias G., Ferre-Borrull J., Pallares J., Marsal L. F., *Photoluminescent enzymatic sensor based on nanoporous anodic alumina.* ACS Appl Mater Interfaces, 2012. **4**(7): p. 3584-3588.

[13] Evans P.R., Yi G., Schwarzacher W., *Current perpendicular to plane giant magnetoresistance of multilayered nanowires electrodeposited in anodic aluminum oxide membranes.* Applied Physics Letters, 2000. **76**(4): p. 481-483.

[14] Huang C.-H., Lin, Hsing-Ying, Tzeng, Yonhua, Fan, Chien-Hsiang, Liu, Chih-Yi, Li, Chia-Yi, Huang, Cheng-Wen. Chen, Nan-Kuang, Chui, Hsiang-Chen, *Optical characteristics of pore size on porous anodic aluminium oxide films with embedded silver nanoparticles.* Sensors and Actuators A: Physical, 2012. **180**: p. 49-54.

[15] Xu, Li, Hua, Zhao, Guang-Yu, Li, Hu-Lin, *Electrodeposition of ferromagnetic nanowire arrays on AAO/Ti/Si substrate for ultrahigh-density magnetic storage devices.* Materials Letters, 2006. **60**(19): p. 2335-2338.

[16] Sulka G.D., Brzózka, Agnieszka, Zaraska, Leszek, Jaskuła, Marian, *Through-hole membranes of nanoporous alumina formed by anodizing in oxalic acid and their applications in fabrication of nanowire arrays.* Electrochimica Acta, 2010. **55**(14): p. 4368-4376.

[17] Schwirn K., Lee, Hillebrand R., Steinhart M., Nielsch K., Gosele U., *Self-ordered anodic aluminum oxide formed by H2SO4 hard anodization.* ACS Nano, 2008. **2**(2): p. 302-310.

[18] M. Almasi Kashi, *The effect of temperature and concentration on the self-organized pore formation in anodic alumina.* Journal of Physics D: Applied Physics, 2005. **38**(14): p. 2396-2399.

[19] Jaroonpak E., Terawan, Porntawee, Wannawong, Naruemon, Kaewrawang, Arkom, Kruehong, Chaiyaput, Thabuth, Mallika, *The Synthesis of Nano-*

Porous Alumina by Anodization Process. Applied Mechanics and Materials, 2015. **781**: p. 235-238.

[20] Keshavarz A., Parang, Zohreh,Nasseri, Ahmad, *The effect of sulfuric acid, oxalic acid, and their combination on the size and regularity of the porous alumina by anodization.* Journal of Nanostructure in Chemistry, 2013. **3**(1): p. 34-37.

[21] Song Y., Jiang, Longfei, Qi, Weixing, Lu, Chao, Zhu, Xufei, Jia, Hongbing, *High-field anodization of aluminum in concentrated acid solutions and at higher temperatures.* Journal of Electroanalytical Chemistry, 2012. **673**: p. 24-31.

[22] Montero-Moreno J.M., Sarret M., Müller C., *Influence of the aluminum surface on the final results of a two-step anodizing.* Surface and Coatings Technology, 2007. **201**(14): p. 6352-6357.

[23] Ghorbani M., Nasirpouri F., Iraji zad A., Saedi A., *On the growth sequence of highly ordered nanoporous anodic aluminium oxide.* Materials & Design, 2006. **27**(10): p. 983-988.

[24] Spooner R.C., *The Anodic Treatment of Aluminum in Sulfuric Acid Solutions.* Journal of The Electrochemical Society, 1955. **102**(4): p. 156-162.

[25] Yu, H.-M., Lee, Jaehyeong, *Fabrication of nanomaterials using anodic aluminum oxide and their properties.* Current Applied Physics, 2011. **11**(1): p. S339-S345.

[26] Lin Y., Lin Q., Liu X., Gao Y., He J., Wang W., Fan Z., *A Highly Controllable Electrochemical Anodization Process to Fabricate Porous Anodic Aluminum Oxide Membranes.* Nanoscale research letters, 2015. **10**(1): p. 495-506.

[27] Chiu R.-L., Chang, Peng-Heng, Tung, Chih-Hang, *The effect of anodizing temperature on anodic oxide formed on pure Al thin films.* Thin Solid Films, 1995. **260**(1): p. 47-53.

[28] Kashi M.A., Ramazani A., Raoufi M., Karimzadeh A., *Self-ordering of anodic nanoporous alumina fabricated by accelerated mild anodization method.* Thin Solid Films, 2010. **518**(23): p. 6767-6772.

[29] Chahrour K.M., Ahmed, Naser M., Hashim M. R., Elfadill, Nezar G., Maryam W., Ahmad M. A., Bououdina M., *Effects of the voltage and time of anodization on modulation of the pore dimensions of AAO films for*

nanomaterials synthesis. Superlattices and Microstructures, 2015. **88**: p. 489-500.

[30] Qin X., Zhang, Jinqiong, Meng, Xiaojuan, Deng, Chenhua, Zhang, Lifang, Ding, Guqiao, Zeng, Hao, Xu, Xiaohong, *Preparation and analysis of anodic aluminum oxide films with continuously tunable interpore distances.* Applied Surface Science, 2015. **328**: p. 459-465.

[31] Kikuchi T., Nishinaga, Osamu, Natsui, Shungo, Suzuki, Ryosuke O., *Fabrication of Self-Ordered Porous Alumina via Etidronic Acid Anodizing and Structural Color Generation from Submicrometer-Scale Dimple Array.* Electrochimica Acta, 2015. **156**: p. 235-243.

[32] *AAO Publications*. cited on: 28-09-2016; Available from: http://www.inredox.com/aao-publications/.

[33] Kim H., Popov, Branko N., Chen, Ken S., *A Novel Electrodeposition Process for Plating Zn-Ni-Cd Alloys.* Journal of The Electrochemical Society, 2003. **150**(2): p. 81-88.

[34] Haidopoulos M., Turgeon S., Sarra-Bournet C., Laroche G., Mantovani D., *Development of an optimized electrochemical process for subsequent coating of 316 stainless steel for stent applications.* Journal of materials science. Materials in medicine, 2006. **17**(7): p. 647-657.

[35] Lee E.S., *Machining Characteristics of the Electropolishing of Stainless Steel (STS316L).* The International Journal of Advanced Manufacturing Technology, 2000. **16**(8): p. 591-599.

[36] Barillaro G., Nannini A., Piotto M., *Electrochemical etching in HF solution for silicon micromachining.* Sensors and Actuators A: Physical, 2002. **102**(1-2): p. 195-201.

[37] V. P. Parkhutik, *Theoretical modelling of porous oxide growth on aluminium.* Journal of Physics D: Applied Physics, 1992. **25**(8): p. 1258-1263.

[38] Tsangaraki-Kaplanoglou I., Theohari S., Dimogerontakis, Wang, Yar-Ming, Kuo, Hong-Hsiang, Kia, Sheila, *Effect of alloy types on the anodizing process of aluminum.* Surface and Coatings Technology, 2006. **200**(8): p. 2634-2641.

[39] Bogar F.D., Foley R. T., *The Influence of Chloride Ion on the Pitting of Aluminum.* Journal of The Electrochemical Society, 1972. **119**(4): p. 462.

[40] Nguyen T.H., Foley R. T., *On the Mechanism of Pitting of Aluminum.* Journal of The Electrochemical Society, 1979. **126**(11): p. 1855-1860.

[41] Epstein A.J., Smallfield J. A. O., Guan H., Fahlman M., *Corrosion protection of aluminum and aluminum alloys by polyanilines: A potentiodynamic and photoelectron spectroscopy study.* Synthetic Metals, 1999. **102**(1-3): p. 1374-1376.

[42] Bradford S., *Corrosion Control*. 2nd ed. 1993, Canada: CASTI Publishing Inc. 141.

[43] Trethewey K.R., Chamberlain J., *Corrosion for science and engineering*. 2nd ed. 1995, United States: NACE International, Houston, TX (United States). 466.

[44] Lin J.S., Chen, Shih Hsun, Huang, Ker Jer, Hun, Chien Wan, Chen, Chien Chon, *Challenges to Fabricate Large Size-Controllable Submicron-Structured Anodic-Aluminum-Oxide Film.* Atlas Journal of Materials Science, 2015. **2**(2): p. 65-72.

[45] Fontana M.G., *Corrosion Engineering*. 3rd ed. 2005, Singapore: Tata McGraw-Hill. 556.

[46] Li Q., *Liquid Crystals Beyond Display*. 1st ed. 2012, Canada: John Wiley & Sons. 587.

[47] Bahadur B., *Liquid Crystals: Applications and Uses*. 1st ed. Vol. 1. 1995: World Scientific. 21.

[48] Hussain Z., Qazi F., Ahmed M. I., Usman A., Riaz A., Abbasi A. D., *Liquid crystals based sensing platform-technological aspects.* Biosensors & bioelectronics, 2016. **85**: p. 110-127.

[49] Hu, Q.-Z., Jang, Chang-Hyun, *Liquid crystal-based sensors for the detection of heavy metals using surface-immobilized urease.* Colloids and Surfaces B: Biointerfaces, 2011. **88**(2): p. 622-626.

[50] Peter John K., Sheikh S.T., *Anodizing of Aluminum with improved Corrosion Properties.* Journal of chemical society, 2010. **32**(1): p. 46-51.

[51] O. Jessensky, *Self-Organized Formation of Hexagonal Pore Structures in Anodic Alumina.* Electrochemcial Society, 1998. **145**(11): p. 3735-3740.

[52] Budimanz D, *Fabrication and Characterization of Porous Anodic Alumina Films from Impure Aluminum Foils.* Electrochem. Soc, 2007. **154**(1): p. 60-66.

[53] Fang X., Wu L., *Handbook of Innovative Nanomaterials: From Syntheses to Applications*. 1st ed. 2012: Pan Stanford Publishing. 960.

[54] Nalwa H.S., *Encyclopedia of Nanoscience and Nanotechnology*. 2nd ed. 2003: American Scientific Publishers. 6000.

[55] Eftekhari A., Alkire R.C., Gogotsi Y., Simon P., *Nanostructured Materials in Electrochemistry*. 1st ed. 2008: Wiley.

[56] Rocca E., Vantelon, Delphine, Reguer, Solenn, Mirambet, François, *Structural evolution in nanoporous anodic aluminium oxide.* Materials Chemistry and Physics, 2012. **134**(2-3): p. 905-911.

[57] Akiya S., Kikuchi, Tatsuya, Natsui, Shungo, Suzuki, Ryosuke O., *Optimum Exploration for the Self-Ordering of Anodic Porous Alumina Formed via Selenic Acid Anodizing.* Journal of The Electrochemical Society, 2015. **162**(10): p. 244-250.

[58] Lee W., Nielsch K., Gösele U., *Self-ordering behavior of nanoporous anodic aluminum oxide (AAO) in malonic acid anodization.* Nanotechnology, 2007. **18**(47): p. 475713.

[59] Zaraska L., Jaskuła, Marian, Sulka, Grzegorz D., *Porous anodic alumina layers with modulated pore diameters formed by sequential anodizing in different electrolytes.* Materials Letters, 2016. **171**: p. 315-318.

[60] Akiya S., Kikuchi, Tatsuya, Natsui, Shungo, Sakaguchi, Norihito, Suzuki, Ryosuke O., *Self-ordered Porous Alumina Fabricated via Phosphonic Acid Anodizing.* Electrochimica Acta, 2016. **190**: p. 471-479.

[61] Takenaga A., Kikuchi, Tatsuya, Natsui, Shungo, Suzuki, Ryosuke O., *Exploration for the Self-ordering of Porous Alumina Fabricated via Anodizing in Etidronic Acid.* Electrochimica Acta, 2016. **211**: p. 515-523.

[62] Rahman M.M., Garcia-Caurel E., Santos A., Marsal L. F., Pallares J., Ferre-Borrull J., *Effect of the anodization voltage on the pore-widening rate of nanoporous anodic alumina.* Nanoscale Research Letters, 2012. **7**(1): p. 474-480.

[63] Li Y., Ling Z. Y., Chen S. S., Wang J. C., *Fabrication of novel porous anodic alumina membranes by two-step hard anodization.* Nanotechnology, 2008. **19**(22): p. 604-609.

[64] Masuda H., Yamada, Haruki, Satoh, Masahiro, Asoh, Hidetaka, Nakao, Masashi, Tamamura, Toshiaki, *Highly ordered nanochannel-array*

architecture in anodic alumina. Applied Physics Letters, 1997. **71**(19): p. 2770-2772.

[65] Surawathanawises K., Cheng X., *Nanoporous anodic aluminum oxide with a long-range order and tunable cell sizes by phosphoric acid anodization on pre-patterned substrates.* Electrochim Acta, 2014. **117**: p. 498-503.

[66] Montero-Moreno J.M., Sarret M., Müller C., *Self-ordered porous alumina by two-step anodizing at constant current: Behaviour and evolution of the structure.* Microporous and Mesoporous Materials, 2010. **136**(1-3): p. 68-74.

[67] Losic D., Santos, Abel, *Nanoporous Alumina_ Fabrication, Structure, Properties and Applications*. 1st ed. Vol. 219. 2015: Springer.

[68] Poinern G.E.J., Ali, Nurshahidah, Fawcett, Derek, *Progress in Nano-Engineered Anodic Aluminum Oxide Membrane Development.* Materials, 2011. **4**(12): p. 487-526.

[69] Zaraska L., Sulka, Grzegorz D., Szeremeta, Janusz, Jaskuła, Marian, *Porous anodic alumina formed by anodization of aluminum alloy (AA1050) and high purity aluminum.* Electrochimica Acta, 2010. **55**(14): p. 4377-4386.

[70] Mohajeri M., Akbarpour, Hamed, *Knowledge-based prediction of pore diameter of nanoporous anodic aluminum oxide.* Journal of Electroanalytical Chemistry, 2013. **705**: p. 57-63.

[71] Zhao, Shi, Li, Zhao, Du, *Effects of anodizing conditions on anodic alumina structure.* Journal of Materials Science, 2006. **42**: p. 3878-3882.

[72] Zhao Y.C., Zhang, Xu, Liu W, *A facile approach to formation of through-hole porous anodic aluminium oxide film.* Materials Letters, 2005. **59**(1): p. 40-43.

[73] Zhao, Jiang, Xiao-Xue, Shi, Chun-Sheng, Li, Jia-Jun, Zhao, Zhi-Guo, Du, Xi-Wen, *Effects of anodizing conditions on anodic alumina structure.* Journal of Materials Science, 2007. **42**(11): p. 3878-3882.

[74] De Azevedo, Khoury H.J., de Vasconcelos E.A.; Da Silva E.F. Jr., *Spectroscopic characteristics of doped nanoporous aluminium oxide.* Materials Science and Engineering, 2004: p. 171-174.

[75] Shingubara S., *Fabrication of Nanomaterials Using Porous Alumina Templates.* Journal of Nanoparticle Research, 2003. **5**(1/2): p. 17-30.

[76] Ono S., Masuko, Noboru, *Evaluation of pore diameter of anodic porous films formed on aluminum.* Surface and Coatings Technology, 2003. **169–170**: p. 139-142.

[77] Smallman R.E., Bishop R.J., *Modern Physical Metallurgy and Materials Engineering*. 3rd ed. 1999: Elsevier Science.

[78] Carlton R.J., Hunter J. T., Miller D. S., Abbasi R., Mushenheim P. C., Tan L. N., Abbott N. L., *Chemical and biological sensing using liquid crystals.* Liquid Crystals Reviews, 2013. **1**(1): p. 29-51.

[79] Md Jani A.M., D. Losic, and N.H. Voelcker, *Nanoporous anodic aluminium oxide: Advances in surface engineering and emerging applications.* Progress in Materials Science, 2013. **58**(5): p. 636-704.

[80] Birbilis N., Buchheit R. G., *Electrochemical Characteristics of Intermetallic Phases in Aluminum Alloys: An Experimental Survey and Discussion.* Journal of The Electrochemical Society, 2005. **152**(4): p. 140-151.

[81] Budiman, R. Arief, *Fabrication and Characterization of Porous Anodic Alumina Films from Impure Aluminum Foils.* Journal of The Electrochemical Society, 2007. **154**(1): p. 60-66.